HHS Public Access

Author manuscript

Int J Hyperthermia. Author manuscript; available in PMC 2016 March 01.

Published in final edited form as:

Int J Hyperthermia. 2015 March ; 31(2): 145–162. doi:10.3109/02656736.2015.1007538.

Histotripsy Methods in Mechanical Disintegration of Tissue: Toward Clinical Applications

VA Khokhlova[1,2], **JB Fowlkes**[3,4], **WW Roberts**[4,5], **GR Schade**[6], **Z Xu**[4], **TD Khokhlova**[7], **TL Hall**[4], **AD Maxwell**[1,6], **YN Wang**[1], and **CA Cain**[4]

[1]Center for Industrial and Medical Ultrasound, Applied Physics Laboratory, University of Washington, 1013 NE 40th Street, Seattle, WA 98105, USA

[2]Department of Acoustics, Physics Faculty, Moscow State University, Moscow 119991, Russia

[3]Department of Radiology, University of Michigan, 3226C Medical Sciences Building I, 1301 Catherine Street, Ann Arbor, MI 48109-5667

[4]Department of Biomedical Engineering, University of Michigan, 1107 Carl A. Gerstacker Building, 2200 Bonisteel Blvd., Ann Arbor, MI 48109-2099

[5]Department of Urology, University of Michigan, 3879 Taubman Center, 1500 East Medical Center Dr., Ann Arbor, MI 48109-5330

[6]Department of Urology, University of Washington Medical Center, 1959 NE Pacific Street, Box 356510, Seattle, WA 98195, USA

[7]Department of Gastroenterology, University of Washington Medical Center, 1959 NE Pacific Street, Box 356510, Seattle, WA 98195, USA

Abstract

Purpose—In high intensity focused ultrasound (HIFU) therapy, an ultrasound beam is focused within the body to locally affect the targeted site without damaging intervening tissues. The most common HIFU regime is thermal ablation. Recently, there has been increasing interest in generating purely mechanical lesions in tissue (histotripsy). This paper provides an overview of several studies on the development of histotripsy methods toward clinical applications.

Material and Methods—Two histotripsy approaches and examples of their applications are presented. In one approach, sequences of high-amplitude, short (microsecond-long), focused ultrasound pulses periodically produce dense, energetic bubble clouds that mechanically disintegrate tissue. In an alternative approach, longer (millisecond-long) pulses with shock fronts generate boiling bubbles and the interaction of shock fronts with the resulting vapor cavity causes tissue disintegration.

Results—Recent pre-clinical studies on histotripsy are reviewed for treating benign prostatic hyperplasia (BPH), liver and kidney tumors, kidney stone fragmentation, enhancing antitumor

Telephone: +1-734-763-5882 (Brian Fowlkes), fowlkes@umich.edu. Telephone: +1-206-221-6585 (Vera Khokhlova), vera@apl.washington.edu.

Drs. J. B. Fowlkes, W.W. Roberts, Z. Xu, T. L. Hall, and C. A. Cain have financial interest and/or other relationship with HistoSonics.

immune response, and tissue decellularization for regenerative medicine applications. Potential clinical advantages of the histotripsy methods are discussed.

Conclusions—Histotripsy methods can be used to mechanically ablate a wide variety of tissues, whilst selectivity sparing structures such as large vessels. Both ultrasound and MR imaging can be used for targeting and monitoring the treatment in real time. Although the two approaches utilize different mechanisms for tissue disintegration, both have many of the same advantages and offer a promising alternative method of noninvasive surgery.

Keywords

high intensity focused ultrasound; ultrasound; physics

INTRODUCTION

High intensity focused ultrasound (HIFU) therapy is a relatively new non-invasive medical technology, in which an ultrasound beam is focused within the body to locally affect the targeted site without damaging intervening tissues [1]. Currently, the most common HIFU regime in clinical use is thermal ablation, which has been applied to treat a variety of both benign and malignant tumors including uterine fibroids [2], prostate cancer [3], benign prostate hyperplasia (BPH), liver and kidney tumors [4,5], and bone metastasis [6]. Recently, the first successful surgeries on brain tissue were reported for treating essential tremor and tumors [7, 8]. Unlike other thermal ablation modalities, such as radiofrequency (RF) or laser ablation, HIFU is completely non-invasive. Targeting for the HIFU treatment is usually performed using either magnetic resonance (MR) imaging or B-mode ultrasound imaging; real-time visualization of the treated volume in the clinical systems employs either MR thermometry [2, 6] or observation of the echogenic region on the B-mode images indicating, in most cases, the start of boiling in tissue, when present [4, 5].

Recent studies have shown significant interest in expanding the capabilities of therapeutic ultrasound to generate purely mechanical damage of tissue without thermal coagulation – this approach is named histotripsy. The term “histotripsy”, from histo- tissue [G. *histos*] and -tripsy - to crush [G. *tripsis*] describes the disintegration or liquefaction of tissue by short ultrasound pulses [9] in analogy to lithotripsy. In the approach first pursued by researchers at the University of Michigan (UM), very short (microsecond-long), intense acoustic pulses repeated with low duty factor periodically produce dense energetic bubble clouds in tissue. The repeated expansion and contraction of the bubble clouds mechanically disintegrate tissue to a subcellular level, generating non-thermal lesions. An alternative approach to mechanically disintegrate (liquefy) tissue using high amplitude ultrasound has been proposed in collaborative studies between the University of Washington in Seattle (UW) and Moscow State University (MSU) in Russia [10]. This method, termed boiling histotripsy, uses longer (millisecond instead of microsecond) duration focused ultrasound pulses to rapidly generate a millimeter-sized boiling bubble (instead of a cavitation cloud). This is achieved through tissue heating due to the strong attenuation of the ultrasound energy at the shock fronts that form naturally in the acoustic waveform by nonlinear propagation effects [11]. Interaction of these shock fronts with the resulting vapor cavity causes tissue disintegration into subcellular debris.

Histotripsy approaches may have certain clinical advantages over traditional HIFU including ultrasound imaging of treatment in real-time, avoiding overheating of intervening tissues, natural passage or easier resorption of the fragmented tissue, and a broader spectrum of potential bioeffects in tissue. Some of these attributes are discussed later in the paper after brief description of the two approaches given below.

Cavitation cloud histotripsy is a highly nonlinear and threshold phenomenon where bubble cloud activation does not migrate and lesion boundaries can be seen bisecting individual cells [12] (Figure 1). The region over which the bubble cloud is activated is constrained to within the portion of the focal zone exceeding this threshold where the amplitude outside this region is insufficient to sustain this cavitational activity thus preventing migration. The dense bubble clouds found to cause histotripsy are only initiated at the focus whenever the peak negative pressure in acoustic waveform exceeds an “intrinsic threshold”, which is around 28 MPa for most soft tissues [13, 14]. This threshold is characterized by the consistent formation of a dense bubble cloud unlike typical acoustic cavitation that might be more sparsely distributed in a lower amplitude pressure field. Reduced peak negative pressure half-cycles (< 28 MPa) cannot directly initiate the dense clouds for histotripsy. Additional information on the relationship among various thresholds is provided in the discussion. There are two approaches to exceeding the intrinsic threshold for the purposes of histotripsy: shock scattering and direct excitation. Nonlinear propagation readily forms pulses with peak rarefactional pressure (p_-) values in the range of 12 MPa to 25 MPa (less than the intrinsic threshold) and positive shock fronts with peak pressures (p_+) greater than 50 MPa. In the shock scattering approach [15], the initial negative half cycle initiates sparsely distributed incidental bubbles in the focus. For pulses exceeding 3 cycles, subsequent positive shock fronts are inverted at the pressure release bubble boundary and the inverted shock front can exceed the intrinsic threshold, inducing a dense bubble cloud from the scattered now-negative pressure waveform. With subsequent cycles, shock fronts produce supra-intrinsic threshold regions by reflecting from the enlarging dense bubble cloud growing towards the transducer. The growth of the bubble cloud continues for ~10 cycles until the intensity boundaries are reached where this shock scattering process no longer exceeds the intrinsic threshold; longer excitations produce rapidly diminishing effects. If any part of the primary pulse exceeds the intrinsic threshold [13], a dense bubble cloud capable of histotripsy is directly generated, even with a single negative half cycle. It is therefore attractive to classify different cavitation cloud histotripsy approaches by the length of the waveforms necessary to produce the desired lesions. “Intrinsic threshold histotripsy” can use pulses consisting of only a single negative pressure “half-cycle” pulse with the peak pressure exceeding about 28 MPa. The pulse can be as short as several hundred nanoseconds or less when synthesized as a monopolar pulse as will be discussed later. “Shock scattering histotripsy” can be produced by pulses from 3 to 10 cycles (several microseconds to about 20 microseconds) of 0.5 – 1.0 MHz frequency, where, as explained above, the combination of peak negative cycles ranging from about 12 MPa to 25 MPa combine with reflections of the essential positive shock fronts exceeding about 50 MPa. In both cases, thermal effects are negligible if a low pulse repetition rate (<1%) is used.

The boiling histotripsy approach uses sequences of much longer HIFU pulses (millisecond instead of microsecond duration, see Figure 1) and initiation of localized boiling as opposed to cloud cavitation [16]. It has been shown that shock fronts generated from nonlinear propagation effects in the focal region of the HIFU beam effects are superfocused and are present in a small subvolume within the focal region, much smaller than the focal region of the linearly focused beam [17]. These shock fronts heat tissue tens of times more rapidly compared to the harmonic waves of the same amplitude. Shock wave heating results in a temperature increase to over 100°C and initiation of localized boiling at the focus in as short as a few milliseconds [18]. The boiling bubble rapidly grows to a size exceeding the small subvolume heated by shocks and cools to form a vapor cavity. The heated and potentially thermally ablated region in tissue is much smaller than the volume occupied by the vapor cavity it creates. Following vapor cavity formation, shock fronts from the rest of the pulse interact with the tissue – vapor cavity interface to generate ultrasonic micro-fountains and tissue atomization: the emission of liquid droplets and tissue micro-fragments that fill the cavity [19]. If the HIFU pulse is not much longer than the time-to-boil, thermal effects in the resulting lesion are negligible compared to the mechanical disintegration caused by the exploding bubble and its interaction with the acoustic pulse [20]. Peak pressures required for boiling histotripsy are typically lower than in cavitation cloud histotripsy, which enables the use of currently available HIFU clinical systems; however, extra energy capacity is required to generate longer pulses. A typical pulsing protocol of 2-MHz frequency, 70 MPa shock-front amplitude at the focus, 10 ms pulse duration, 1% duty factor was found to produce purely mechanical single lesions in *ex-vivo* bovine liver tissue (Figure 1), kidney, and heart, as well as in porcine liver *in vivo* [16, 20, 21].

A detailed comparison of the two methods, termed cavitation-cloud histotripsy and boiling histotripsy for the purposes of this review, examining the ultrasound field parameters, exposures, and physical mechanisms of tissue disintegration was published in the recent joint paper of the researchers from UM, UW, and MSU [22]. The present paper provides an overview of some recent studies related to the development of these technologies toward clinical applications.

CAVITATION CLOUD HISTOTRIPSY

Histotripsy of Prostate

Histotripsy is a promising technique for the treatment of prostate diseases, specifically benign prostatic hyperplasia (BPH) and prostate cancer. BPH is a common condition that arises from prostate enlargement and compression of the urethra (which passes through the center of the prostate). This commonly produces lower urinary tract symptoms (LUTS): urinary frequency, urgency, intermittency, incomplete emptying, weak stream, straining, and nocturia [23]. BPH can also lead to more dangerous conditions, including urinary retention, urinary tract infection, hematuria, bladder calculi, and renal insufficiency. Approximately 50% of men in their 50’s and 80% of men in their 80’s are affected [24, 25]. This high prevalence and the associated deterioration in quality of life result in approximately 4.5 million physician visits annually for a primary diagnosis of BPH among men in the United States [26].

The current gold standard therapy for BPH is transurethral resection of the prostate (TURP), a surgical procedure where tissue is mechanically removed to debulk the overgrown adenomatous tissue in the center of the prostate and create a wider urinary channel. Unfortunately, TURP is associated with an 18% complication rate and a 0.2–1.5% mortality rate [24, 27, 28]. Modern variations of transurethral resection include electrovaporization, laser vaporization, and laser enucleation techniques. Radiofrequency ablation (TUNA), microwave therapy (TUMT), and interstitial laser therapy were developed as minimally invasive alternatives to lessen the morbidity and mortality of TURP but have not been as effective or durable. Histotripsy may provide a less invasive alternative therapy that utilizes extracorporeal energy delivery, real-time ultrasound imaging feedback, and mechanical homogenization of targeted tissue to reproduce the debulking accomplished with TURP but with lower morbidity.

To examine the utility of prostate histotripsy, a canine model using older intact canine subjects was developed owing to the anatomic similarity to the human prostate. Transabdominal application of histotripsy was facilitated by placing a water bag over the suprapubic region of anesthetized canine subjects positioned supine. The histotripsy transducer focus was targeted on the canine prostate and coupled through the water bolus (Figure 2). Real-time image feedback for targeting and monitoring of treatment was accomplished by using a transrectal 10 MHz ultrasound imager. The cavitation bubble cloud was easily identified as a hyperechoic focus on the image. Translation of the transducer allowed for volume ablation by “driving” the bubble cloud through the region of interest within the prostate.

The feasibility of prostate histotripsy was initially established in acute canine subjects using a 750 kHz transducer with pulse repetition frequency (PRF) of 100-500 Hz (duty cycle < 0.4%) [29]. It was apparent that the more dense periurethral tissue required a greater number of pulses (270,000 pulses/cm^3 vs. 28,000 pulses/cm^3) to disintegrate than glandular tissue [30]. An alternative to replicating the anatomic result of TURP is to spare the urethra and treat just the surrounding glandular tissue. When this approach was applied - targeting 1-2 cm^3 volumes of glandular tissue - prostate volume decreased by 12%, eight weeks after treatment, without abscess formation or chronic inflammation [31].

During the course of these experiments it was apparent that there was very little bleeding. To examine this more directly, an anticoagulant (warfarin, international normalized ratio 1.2-11.3) was administered to nine canine subjects before being treated with an aggressive histotripsy protocol to create a substantial TURP-like defect within the prostate [32]. Only mild hematuria without clots was observed during the first 48 hours after treatment, consistent with previous studies. In addition, systemic measurement of hemoglobin did not decrease, consistent with minimal blood loss.

To evaluate the local and systemic effects of histotripsy, eighteen canine subjects underwent treatment of a 4 cm^3 volume of prostate, encompassing glandular tissue and prostatic urethra. When prostates were harvested 0 to 56 days after treatment, a well-demarcated treatment cavity was apparent. Only mild post-treatment discomfort, assessed with a validated pain instrument, was observed and resolved shortly after urinary catheter removal

[33]. Modest transient post-treatment abnormalities in blood tests were observed, consistent with anesthesia administration and tissue ablation [34]. Healing was evident by urothelialization of the treatment cavity with minimal residual debris 28 days after treatment. From this study, it was concluded that histotripsy could be applied safely and was well tolerated in the canine model.

The prostate is surrounded by critical structures that are responsible for urinary continence and erectile function. To establish the thresholds for damage of these critical periprostatic structures, studies were conducted applying 750,000 histotripsy pulses to the bladder trigone, and ureteral orifices and 1000, 10000, or 100000 pulses directly to the rectum, urinary sphincter, and neurovascular bundles [35, 36]. Moderate collagen disruption and focal mucosal homogenization was seen in the rectum with 10,000 pulses, representing the lowest threshold for damage (equivalent to glandular prostate tissue). However, the other critical structures were resilient to histotripsy damage even after application of 100,000 pulses. Interestingly, the blood vessels and nerves within the neurovascular bundles were structurally intact, though extensive homogenization was apparent in adjacent fat and loose connective tissue [35].

Prostate cancer is another condition that may be uniquely suited to histotripsy. Ten canine subjects underwent implantation of malignant ACE-1 cells into their prostates [37]. After ultrasound confirmation of tumor growth, histotripsy was applied. Harvesting of prostates revealed tumor homogenization in acute subjects while histology from chronic subjects revealed hemorrhage and necrosis. Interestingly, metastases were apparent in all three tumor-implanted controls, while none of the histotripsy-treated chronic subjects exhibited metastases [37].

These first studies propose that histotripsy, due to its distinct process of cavitational tissue ablation and unique features (extracorporeal energy delivery, real-time visualization of homogenization, and echogenic change with treatment) has great potential as a treatment for BPH and prostate cancer.

Liver Cancer Application

Hepatocellular carcinoma (HCC) has been the fastest growing cancer in the United States over the last decade [38]. While liver transplantation may be curative, only a small patient population receives this treatment [39]. Surgical resection has a high morbidity, death rate of 1-5% and is contraindicated in patients with decompensated cirrhosis [40]. Radiofrequency ablation (RFA) has become a standard therapy for tumors <3 cm diameter with fewer than three tumor nodules [40]. Other thermal ablation techniques include microwave- [41], cryo- [42], and laser- [43] therapy. As blood flow through the highly vascular liver creates a natural “heat sink”, thermal-based minimally invasive ablation methods suffer from inconsistent ablation, ineffective ablation for tumors near major vessels, and extensive treatment times for tumors larger (>3 cm dia.) [44-46]. These ablation modalities do not have reliable imaging feedback during treatments. HIFU ablation for liver cancer therapy does not require device insertion, is guided by real-time ultrasound [4,5] or magnetic resonance imaging (MRI) [47], and has the potential to treat multiple and larger tumors. However, HIFU treatment still suffers from the heat sink effect along with the challenge to

overcome the rib obstruction. As ribs are highly absorptive, skin burns and subcostal edema have been reported in clinical HIFU liver ablation cases [4, 48, 5]. Respiration-induced motion also significantly compromises the treatment precision and efficacy [47].

Histotripsy can produce consistent and fast disintegration of tissue with various heat dissipation patterns, even when the tissue is in proximity to major vessels. The disintegration is often self-limited at the boundaries of major vessels with surrounding tissue completely homogenized. The therapy focus can be scanned to treat a large tumor volume (>3cm) and multiple nodules. As noted in the previous section, cavitation bubbles can be visualized with ultrasound imaging, allowing precise targeting. The change in tissue during treatment can be also be directly monitored using standard imaging modalities such as ultrasound and MRI, which allows histotripsy to be guided in real-time [49, 50]. For transthoracic liver ablation, ribs in the ultrasound pathway cause periodic blockage of ultrasound, resulting in a significantly decreased focal pressure and increased grating lobe pressure levels [51-53]. By applying appropriate pressure amplitude where the focal pressure is above the histotripsy threshold while the grating lobe pressure is not, a confined cloud at the focus and a precise lesion can be produced despite the intervening ribs [54, 55]. Thermal damage to the overlying and surrounding tissue is prevented by using prolonged cooling times between pulses (i.e. a low duty factor). The following is an overview of the feasibility of developing histotripsy for non-invasive liver ablation in an *in vivo* porcine liver model with size and anatomy similar to human [56, 57].

First experiments studied the *in vivo* feasibility for creating precise lesions through ribs and overlying tissue. Twelve ~1 cm^3 lesions were successfully created with locations spanning the entire liver, including the superior and inferior regions of the left, middle, and right lobes [56]. Histotripsy pulses of 1 MHz, 10 cycles, 500 Hz PRF, and 14-17 MPa linearly estimated *in situ* peak negative pressure (p_-) were applied. Treatments were performed in 16.7 minutes through 3-6.5 cm of overlying tissue with the rib cage covering 30-50% (including intercostal space) of the transducer aperture. Histological evaluation of histotripsy lesions showed complete fractionation of hepatic parenchyma inside the treated volume with sharp boundaries of partially ablated liver tissue <500 μm for all treatments.

In a second set of experiments, tissue-selective ablation and large volume ablation were investigated. Two lesions up to 60 cm^3 were generated in the livers of two pigs using the same histotripsy parameters used for the first study. The liver tissue, vessels, gallbladder, and other tissues within and surrounding the treatment region were evaluated histologically for any damage. Two liver volumes of 18 cm^3 and 60 cm^3 were liquefied *in vivo* within 60 minutes by mechanically steering the focus [56]. Histotripsy-induced liver liquefaction was self-limited at the boundaries of critical structures including the major vessels and gallbladder. Liver tissue surrounding major vessels was completely disintegrated, yet the vessels larger than 300 μm remained intact (Figure 3).

A third experiment studied the effect of rib obstruction without using aberration correction. Histotripsy liver ablations were conducted in 8 pigs with 4 lesions generated through transcostal windows with full ribcage obstruction and through transabdominal windows without rib coverage. Treatments were performed with a 750 kHz focused transducer using

5 cycle pulses at 200 Hz PRF with linearly estimated *in situ* p_- of 13-17 MPa. Temperatures on overlying tissues including the ribs were measured with needle thermocouples inserted subcutaneously. Treatments of approximately 40 minutes were applied, allowing overlying tissue temperatures to reach an equilibrium. Lesions yielded statistically comparable ablation volumes of 3.6±1.7 cm^3 and 4.5±2.0 cm^3 in treatments with full ribcage coverage (transcostal) and no rib obstruction (transabdominal), respectively. The average temperature increase in transcostal treatments was 3.9±2.1 ºC, while transabdominal treatments showed an increase of 1.7±1.3 ºC. No damage was seen on the ribcage or other overlying tissues [55].

The results of these studies demonstrated that histotripsy created precise lesions at locations throughout the entire liver through ribs and overlying tissue without using aberration correction. Bubble clouds were successfully initiated and lesions were formed in all treatments. The different heat dissipation associated with regions containing different vascular patterns did not affect the consistency of histotripsy liver ablation. As major vessels and gallbladder have higher mechanical strength and are more resistant to histotripsy [57], the liver surrounding these structures was completely disintegrated while the major hepatic vessels and gallbladder remained intact.

Thrombolysis Application

Thrombosis is the medical term used to describe blood clot formation, the key mechanism behind many cardiovascular diseases. For example, deep vein thrombosis (DVT) affects two million people [58] and causes at least 100,000 deaths annually in the United States alone [59]. Current treatment methods for thrombosis include thrombolytic drugs and catheter-based surgical procedures. Thrombolytic drugs are often ineffective, have a long treatment time, and can cause excessive bleeding, which may be fatal in a small number of cases [60]. Catheter-based procedures are more effective, but they are invasive and carry an increased risk of bleeding, vessel damage, and infection [61]. Ultrasound can be combined with thrombolytic drugs and/or contrast agents to accelerate thrombolysis by enhancing the delivery of drugs into the clot [62]. Despite early signs of success [63], ultrasound assisted thrombolysis is still quite slow (several hours) and carries the similar adverse effects of thrombolytic drugs. To further shorten the treatment time and eliminate the need for thrombolytic drugs, some researchers have investigated thrombolysis via inertial cavitation using ultrasound alone [64, 65] or combined with contrast agents [66, 67].

Histotripsy also uses focused transcutaneous ultrasound, but does not incorporate thrombolytic agents. Instead, the cavitation cloud [68, 69] causes direct mechanical breakdown of the thrombus into acellular debris [70]. Our study shows that clot lysis and blood flow restoration can be achieved at a speed an order of magnitude faster than any current method, without vessel penetration or hazardous embolization. We have investigated the *in vitro* and *in vivo* feasibility of using histotripsy for non-invasive thrombolysis [71-74].

Initial work investigated the effects of histotripsy on blood clots formed *in vitro* from fresh canine blood and $CaCl_2$. Clots were treated using a 1-MHz transducer delivering 5-cycle pulses at 1 kHz pulse repetition rate and $p-$ varying between 2 – 12 MPa [71]. The broken clot fragments were serially filtered through 1 mm, 100 μm, 20 μm, and 5 μm filters after

treatment to measure the total weight of particles in a range of size categories. Histotripsy thrombolysis only occurred at $p_- \geq 6$ MPa when initiation of a cavitating bubble cloud was detected using acoustic backscatter monitoring [75]. Blood clots weighing 330 mg were completely broken down by histotripsy in 1.5 – 5 minutes. There was an increase in thrombolysis rate with p_- between 6-12 MPa (t-test, $P < 0.05$). Filter dry weights changed by ≤ 1 mg suggesting that at least 96% (96 mg of 100 mg) of the particles were smaller than 5 μm.

The *in vivo* feasibility of histotripsy thrombolysis was studied with acute thrombi formed in the femoral vein of juvenile pigs with the same exposure parameters but $p-$ between 14 – 19 MPa [72]. The focus was scanned along the long axis of the vessel to treat the entire extent of the clot observed by B-Mode imaging. To evaluate vessel damage caused by histotripsy alone, vessels without clots were treated for 300 seconds using the same exposure parameters. The bubble cloud was confined to the vessel lumen and appeared on a 2D image as a dynamic echogenic region on the surface of or within the thrombus. The treated area underwent a reduction in echogenicity (10 of 12 cases), indicating thrombolysis was occurring in that region (Figure. 4 A, C & E). In 7 cases, improved flow through the vein was measured by color Doppler (Figure. 4 B, D & F). The mean ultrasound exposure time for a treatment was 10.5 +/− 5.5 minutes for clot length of 20.1 +/− 6 mm and vein inner diameter of 5.5 +/− 1.0 mm. Vessel histology showed denudation of vascular endothelium and small pockets of hemorrhage in the vessel adventitia, underlying muscle and fatty tissue, but perforation of the vessel wall was never observed. In the two instances where histotripsy was not successful, a bubble cloud could not be generated likely due to air trapped in the water bath at the coupling interface with the skin surface and/or within the vessel during catheterization to form the clots.

Finally, a non-invasive embolus trapping (NET) technique was investigated [73, 74]. A cavitation cloud generated in a vessel-flow phantom, similar to that described by Ryan and Foster [76], resulted in two vortices on either side of the cloud. Particles from a clot were trapped in the vortices and simultaneously disintegrated [73]. To evaluate the trapping capability of NET quantitatively, the maximum trapping velocity was measured as a function of $p-$ and PRF, which was defined in [74] by the maximum mean fluid velocity at which a 3-4 mm particle was trapped by the histotripsy-induced cavitation cloud in a 6 mm diameter vessel phantom. The maximum trapping velocity increased linearly with $p-$ and increased as the square root of pulse length and PRF. A 3 mm clot-mimicking particle could remain trapped under a background velocity of 9.7 cm/s and clot fragments treated by NET resulted in debris particles < 75 μm.

These experiments demonstrate the *in vitro* and *in vivo* feasibility of using histotripsy via cavitation alone for thrombolysis. Histotripsy has the potential to overcome the limitations of current thrombolysis methods requiring thrombolytic drugs and/or catheter-based procedures. In addition, the results show that histotripsy can dissolve clots at a rate significantly faster than drugs. Such a therapy would also require less time and lower cost than a surgical catheter. In all cases where a bubble cloud could be initiated in an *in vivo* vessel, at least partial breakdown of the thrombus was achieved. Recanalization of the vessel was not always achieved, in part due to limited resolution of the therapy guidance

transducer, which was not optimized for the DVT study. While vessel perforation was not observed in any of the *in vivo* treatments, small areas of medial and adventitial damage were present in the part of the vessel. This damage should be avoided using a transducer with a smaller focal zone. The clot debris was measured *in vitro* to be no greater than 100 μm, a size unlikely to cause hazardous embolism. In addition, it was found that the cavitating bubble cloud in the vessel can capture, trap, and simultaneously disintegrate a clot fragment flowing through into or near the cavitation cloud.

Kidney Stone Erosion Application

The prevalence of kidney stones is estimated to be 8.8% in the United States [77]. Shock wave lithotripsy (SWL) is a first line non-invasive therapy where high energy acoustic bursts of short duration are applied to fragment a stone so that it can more easily pass from the body. While SWL has been an invaluable tool in the treatment of urinary stones, success rates have been consistently worse than more invasive interventions. SWL fails to achieve stone free status in 20-40% of patients at 3 month follow up [78-80] and even “successful” procedures may involve the painful passage of fragments which have been only partially disintegrated. Large stones (> 20 mm diameter), stones of difficult composition (i.e. cystine), and stones located in the lower pole all have worse outcomes, further discouraging treatment with SWL. Because urinary stones are very common and the problems associated with SWL, there has been a significant research effort to improve SWL. Histotripsy has also shown promise as a method for eliminating stones, where pulse parameters similar to that used in the histotripsy for tissue could be used alone or in combination with current SWL pulses to accelerate stone disruption and reduce fragment size. Additionally control of a wider range of pulse parameters can be used as a research tool for better understanding the mechanisms behind stone comminution.

Pulses similar to that used with histotripsy produce bubble clouds on the surfaces of stones that appear very similar to those seen in SWL [81]. Cavitation bubble clouds produced by either method near a stone surface collapse asymmetrically against the stone. The high-speed flow associated with this collapse is thought to break off small pieces of the stone surface in similar fashion to other instances of cavitation erosion. In practice, histotripsy cavitation erodes the surface of the stone producing very fine debris particles much less than 1 mm in size [82] (Figure 5A).

SWL displays a distinctly different progression of fragmentation beginning with coarse subdivision of a stone (within the first 200 shock waves) followed by gradual reduction of fragment size [83] requiring hundreds to thousands more shock waves. The relative contributions of compressional stress waves and cavitation during SWL are complex and likely to vary during the procedure; however, the surface erosion effect demonstrated through histotripsy would seem to be a dominant effect of cavitation during SWL as well.

Much higher PRFs (up to 1 kHz) have been explored with histotripsy than would be practical with SWL (1 or 2 Hz), producing a far greater number of individual cavitation events in a given amount of time. In these experiments, as the histotripsy pulse rate is increased, the erosion rate also increases but not in a linear fashion. At very high amplitude and PRF, the erosion rate reaches an asymptotic limit (Figure 5B). This is thought to occur

because of a proliferation of remnant cavitation bubbles following the collapse of each histotripsy cavitation cloud. If insufficient time is allowed for these bubbles to dissolve, they may block or reduce the amplitude of a propagating acoustic wave and promote cavitation clouds to collapse away from the stone surface. A similar effect is thought to occur during SWL as well, where the per-shock wave efficiency is known to be significantly worse at 1 Hz than 2 Hz. In experiments where low amplitude acoustic bursts are applied to stimulate coalescence of these remnant bubbles, both the SWL and histotripsy efficiency at higher rates are greatly improved [84, 85]. Optimization of bubble coalescence may shorten the time required for stone comminution procedures or allow for a more thorough treatment.

Very high histotripsy erosion rates have been demonstrated *in vitro* with model stones even for a histotripsy transducer with a relatively small focal zone (Figure 5C). Short bursts of 3-5 acoustic cycles (central frequency of 500 kHz or 1 MHz) at 10 Hz – 1 kHz and peak negative pressures of 10-25 MPa were used to completely erode 10 mm diameter model stones within a few tens of minutes at the highest rates. Thus, the time to completely destroy a stone by histotripsy erosion can be similar to that required by SWL. Using an optimized non-spherically focused source or phased-array scanning techniques may greatly increase the erosion rate. The potential has also been demonstrated for a synergistic combination between histotripsy and lithotripsy. As was previously noted, observations during image-guided clinical procedures and published research have shown lithotripters break primary calculi rapidly, but are much less efficient at reducing these fragments to less than 2 mm – generally requiring hundreds to thousands more shock waves. Non-cavitational mechanisms are thought to become less efficient for smaller fragments leading to a second phase where cavitation must dominate. By interleaving histotripsy bursts within shock waves, a significantly faster stone comminution is achieved where the early subdivision of the stone by shock waves also greatly increases the surface area available to histotripsy erosion (Figure 5C).

The compressional stress component of SWL can be isolated by suppressing cavitation with the use of overpressure [86], performing experiments in non-cavitating fluids such as castor oil [83], or by modifying the shock waveform [87-89]. This work has yielded a good understanding of the specific actions of the shock wave and non-cavitational mechanisms. However, it has only been possible to deduce the role of cavitation in SWL by noting changes in stone comminution when cavitation is suppressed. Using histotripsy, it is possible to isolate the cavitation mechanisms in stone comminution for their direct study. Histotripsy techniques for suppressing unwanted cavitation may also be effective for reducing collateral injury to healthy kidney tissue during SWL or histotripsy procedures [90].

Further research applying histotripsy for the comminution of urinary stones may lead to the development of significantly faster and more reliable techniques. This should improve outcomes for current patients and increase the population of candidates for a non-invasive procedure.

BOILING HISTOTRIPSY

High-output System for Boiling Histotripsy in Liver

As discussed earlier, thermal ablation techniques offer a minimally invasive option for unresectable liver tumors, but complete success can be difficult to achieve because of heat diffusion effects caused by large blood vessels and potential to cause vascular injury. Boiling histotripsy (BH) shows potential as a treatment of solid tumors in the liver, including metastases and hepatocellular carcinoma. Because boiling histotripsy uses such millisecond length pulses to create the bubbles that result in mechanical lesions, minimal heating is applied, thus minimizing potential thermal damage to adjacent tissue structures by heat diffusion or damage to ribs by heating [16]. At a 1% duty cycle, the time-averaged power delivered to the focus is on the order of 1 W. The onset of boiling occurs rapidly enough (10-20 ms) so that BH is unaffected by diffusion and perfusion effects that would result in unanticipated cooling, such as the case of ablation adjacent to a major vessel. Finally, BH has been found to spare tough tissues such as large vessels, while liquefying the surrounding parenchymal mass [20].

Experiments to date have been performed in both *ex vivo* and *in vivo* liver tissues. Preliminary experiments used a degassed water bath with transducers having 1 – 3 MHz operating frequency. Initial experiments were performed near 2 MHz and demonstrated that boiling could be achieved in under 20 ms for focal *in situ* intensities ≥ 11,100 W/cm^2 at a depth of 13.5 mm into the liver [10]. The experimental times required to achieve boiling agreed well with those calculated from hydrophone measurements and nonlinear simulations using the Khokhlov-Zabolotskaya-Kuznetsov (KZK) equation generalized for the nearly linear power law of absorption in tissue. Lesions formed under these conditions produce a ‘tadpole’-shaped lesion, with the head closest to the transducer (Figure 6). The treatment results in complete disintegration of the tissue structure into an acellular liquid with minimal thermal denaturation [20], although in certain cases, the vascular tissue or connective tissue of the hepatic lobules can remain intact. Further studies demonstrated that the tissue effect and lesion shape remain the same using 1, 2, and 3 MHz transducers producing the same shock amplitude at the focus, but the lesion dimensions scaled proportionately to the focal dimensions [16].

The feasibility of using boiling histotripsy *in vivo* has been recently demonstrated in a porcine model [21]. A 2 MHz focused transducer was coupled directly to the exposed liver and used to create single-focus lesions at up to 1.5 cm depth. During exposures, performed under ultrasound image guidance, boiling bubbles appeared on B-mode images as hyperechoic regions with a size that matched the lesion dimensions. It was shown that the lesions generated *in vivo* were similar to those created in *ex vivo* tissue in size and shape.

These results suggest that liver tissue can be effectively disintegrated or liquefied by BH. However, transcutaneous application of BH has yet to be achieved. The preliminary work described above utilized systems with a single-element therapy transducer operated at its maximum power to create lesions at relatively shallow depths. Treatment of liver tumors will require propagating through significant overlying tissue paths and in some cases, with partial blockage by ribs. To address such issues of treating deep tumors, a boiling histotripsy

system was recently developed at the University of Washington [91]. This work incorporates a 15-cm 1 MHz focused transducer that can output pulse-average acoustic power levels as high as 11.5 kW for pulse durations of up to 10 ms (Figure 6A).

In order to evaluate the acoustic output needed to treat tissues at different depths, a derating method has been adopted. This method has been recently developed in a joint effort of researchers from the University of Washington and Moscow State University for nonlinear HIFU fields, including strongly nonlinear focusing conditions and shock front formation [92, 16, 18]. The technique is based on findings, initially demonstrated in simulations, that nearly identical waveforms are produced at the focus in tissue as those in water by adjusting the output pressure of the transducer [92]. As nonlinear effects occur mostly in the small focal region of the beam, where pressure amplitude is the highest, nonlinear distortion of the waveform is minimal along most of the tissue path to the focus. The scaling factor for the source output therefore can be approximated assuming linear wave attenuation over the tissue path. The transducer surface pressure amplitude p_0' needed to produce a focal waveform of certain shape, peak pressures, and shock amplitude at the depth L in tissue follows $p_0' = p_0 \exp(\alpha L)$, where p_0 is the pressure needed to achieve the same waveform in water (without attenuation), α is the linear attenuation coefficient in tissue at the fundamental HIFU frequency.

Preliminary experiments with the new BH system showed that boiling histotripsy lesions could be reliably produced in *ex-vivo* bovine liver above a threshold power of 268 W at 1.8 cm depth, consistent with other studies [16, 20]. The threshold for producing BH lesions was found to increase up to 800 W for generating lesions at 6 cm depth. These results correspond to the derating factor for a source pressure amplitude calculated with attenuation of 0.61 dB/cm at 1 MHz, which is within the reported range of attenuation measured through liver (0.35 – 0.7 dB/MHz/cm) [93] and similar to the results of the earlier studies [18, 20]. Furthermore, the lesion dimensions were consistent at different depths (Figure 6). Given that these experiments only require 7% of the maximum power of the system, boiling histotripsy through substantial overlying tissue paths appears feasible.

Future work is needed to establish treatment through heterogeneous tissue layers that compose the abdominal wall – skin, adipose tissue, and muscle. Furthermore, part of the transducer aperture can be obstructed by ribs which can further increase the power needed to create boiling *in situ* [51, 94]. Provided these conditions can be met, boiling histotripsy may provide a safe therapeutic modality for treatment of tumors in the liver.

Treatment of Renal Carcinoma

Another potential area for adoption of histotripsy methods into clinical use is for focal therapy of small low-stage renal carcinomas (RCC). With a rising incidence over the last few decades, RCC is currently the 6th most common solid organ malignancy in the US, with an estimated 65,140 cases in 2013 [95]. This rise in incidence has also been associated with a stage migration, with >60% of patients now presenting with stage I disease (organ-confined tumors ≤7 cm) [96]. The current standard of care for the majority of these patients is a partial nephrectomy, with the goal of sparing uninvolved kidney to preserve renal

function. While this approach offers excellent oncologic control, it has been associated with complications in up to 25% of patients [97, 100].

With the goal of decreasing morbidity of renal sparing therapies, ablation of small renal cancers has been explored clinically. In the United States, cryo- and radiofrequency-ablation has been adopted into clinical practice. Similar to the situation in the liver, these techniques have been limited to masses <4 cm, due to heat sink effects of renal perfusion [99]. Further, they remain invasive, requiring a percutaneous or laparoscopic approach. Collectively, these factors have contributed to thermal ablation producing inferior oncologic outcomes, yet similar complication rates compared to partial nephrectomy [97].

In Europe and Asia, HIFU thermal ablation of small renal carcinomas has been explored using two different clinical prototype systems. Acute necrosis was reported using a 1.0 MHz clinical prototype system (Storz UTT) in just 9/14 (64%) patients, involving <30% of targeted volume in all cases, whose tumors were treated with HIFU followed by immediate partial nephrectomy in a phase II study [100]. Similarly, the results of HIFU thermal ablation were reported for curative intent in 17 renal tumors using a 0.83 MHz system (HAIFU Chongqing). Of the tumors in which ablation was feasible, only 10/15 (67%) remained free of secondary therapy after 6 months of follow-up with MRI [101]. Similar to cryotherapy and radiofrequency ablation, HIFU ablation of RCC has been limited by uneven heating, due to a combination of tissue properties and heat-sink effects of renal perfusion, and lack of treatment feedback [100]. As a result, an alternative technology to thermal ablation, that offers reliable feedback of treatment could be beneficial.

Towards this goal, histotripsy has been explored as a novel extracorporeal ablative technology for RCC. The feasibility of cavitation cloud histotripsy of renal tissue was demonstrated using an 18-element 750-kHz therapy transducer to deliver 20 μs pulses with a PRF of 100 Hz and linearly estimated $p-$ of 22 MPa in an *in vivo* acute rabbit model [102]. Sonications produced focal disintegration of targeted renal tissues in a dose-dependent fashion with sharp demarcation between treated and untreated renal tissues. Similar to observations in the prostate, the cloud was readily apparent on B-mode ultrasound providing immediate feedback for targeting. Further, histotripsy treatment resulted in loss of tissue echo texture and the appearance of a hypoechoic cavity, which correlates to histologic changes.

In subsequent, chronic rabbit studies, the post-treatment histotripsy cavity was observed to completely resorb with the formation of a small fibrous scar within 60 days of treatment [103]. When used to treat a volume of tissue in *ex vivo* porcine kidneys, the medulla and collecting system were observed to be more resistant to cavitation cloud histotripsy compared to the renal cortex [104]. The ability to target and ablate *in situ* renal tumors was then demonstrated in the implanted VX-2 rabbit papilloma model using a 1 MHz system, 3-cycle pulses ($p-$ ≥20 MPa) at a PRF of 300 Hz using B-mode ultrasound to target tumors [105].

More recently, boiling histotripsy has been evaluated as an alternative histotripsy strategy for renal applications. The seven-element 1-MHz therapy transducer described above and

originally tested for boiling histotripsy in liver was used. The exposure protocol was to deliver 10 ms pulses (*in situ* 98 MPa shock amplitude, peak negative pressure 17 MPa derated from water measurements) at a PRF of 1-3 Hz. *Ex vivo* porcine and human renal tissue has been successfully treated with boiling histotripsy [106]. Morphologically, lesions in both species appear similar progressing from ovoid to “tadpole” shape with dose-dependent mechanical disintegration of targeted tissue that is precise and sharply demarcated between treated and untreated on histological assessment (Figure 7). Lesions generated with PRF of 1 Hz generally had negligible observable thermal effects, while PRF of 3 Hz was associated with some thermal contributions and the generation of a blanched thick paste. Human renal tissue has been observed to be more resistant than porcine tissue, requiring approximately double the number of pulses to produce the same effect. Similar to cavitation cloud histotripsy, renal tissues demonstrate tissue specific sensitivities to the effects of boiling histotripsy, with the cortex demonstrating increased sensitivity to boiling histotripsy compared to the medulla and collecting system in both species. Likewise, boiling histotripsy provides similar feedback on B-mode ultrasound with the appearance of the hyperechoic boiling bubbles at the focus and loss of tissue echo-texture with sufficient pulses.

Collectively, these pre-clinical data suggest an exciting possible clinical application of the histotripsy methods for ablating RCC. Histotripsy ablation of renal tumors would potentially offer a uniquely non-invasive, precise, mechanical treatment of RCC, with real-time imaging feedback to ensure adequate targeting and treatment duration. Future work is needed to optimize delivery of extracorporeal histotripsy to the retroperitoneum within the confines of overlying ribs (acoustic screening) and perinephric fat (attenuation). Such understanding will allow studies aimed at providing insight into the effects of renal histotripsy *in vivo* and ultimately clinical application.

Anti-tumor Immune Response Application

Several studies have reported that thermal HIFU ablation of a primary tumor can potentially activate host anti-tumor immunity [107-109]. It is hypothesized that ablated tumor can improve tumor immunogenicity by releasing tumor-associated antigens, as well as danger-associated molecular patterns (DAMPs) in the form of heat-shock proteins. This release could enhance activation and proliferation of dendritic cells, which, in turn, could lead to the activation of tumor-specific cytotoxic T cells. In terms of the direct effect on tissue, thermal ablation via HIFU would be equivalent to other modes (e.g. radiofrequency or laser ablation), which have also been shown to have an antitumor effect in preclinical studies [110-111].

Histotripsy is hypothesized to be more advantageous for inducing systemic immunity than thermal ablation because it could potentially release large amounts of non-ablated antigens, as well as DAMPs in the form of HMGB1 or ATP. This could be analogous to the administration of immunological vaccines *in situ.* The effects of histotripsy on antitumor immunity were first investigated by a group from Duke University in three different subcutaneous mouse allograft models [112-114]. In these studies, pulsing schemes that closely resemble that of boiling histotripsy (40 ms pulses of 3.3 MHz frequency, 2% duty

factor, reported $p+$= 35 MPa and $p-$=12.5 MPa) were used to create mechanically disintegrated lesions in the subcutaneous tumors, without evident thermal effects. Similar to BH treatments, each lesion corresponded to the appearance of a hyperechoic region in B-mode images, but at the time the mechanism was interpreted as inertial cavitation, and the regime was termed mechanical HIFU or M-HIFU. It was shown that M-HIFU induced enhanced dendritic cells infiltration of tumors and migration to the draining lymph nodes (in murine MC-38 colon adenocarcinoma), suppressed formation of distant metastases (in murine B16 melanoma), and an increase in CD8+ T cell responses (murine prostate cancer RM-9 tumors). As compared to conventional thermal HIFU, M-HIFU was shown to provide superior immunologic responses. However, it was concluded that HIFU-induced lysis alone was likely not sufficient to induce clinically meaningful response, but could serve as a useful adjuvant to other immunotherapy, as well as allow local tumor control.

In recent studies, boiling histotripsy was combined with adoptive T-cell immunotherapy in B16 murine melanoma tumors subcutaneously grafted in C57BL/6J mice [115]. BH treatment (n=8) or sham treatment (n=8) was performed ten days after tumor implantation, when the tumors reached the minimum diameter of 5 mm, exposure parameters were 10 ms pulses of 3.4 MHz frequency, with *in situ* shock amplitude of A_s=66 MPa, $p+$=58 MPa, $p-$=12 MPa, PRF of 1 Hz, and applying 60 pulses per focal spot (Figure 8A). Two days prior to the treatment, adoptive T-cell transfer was performed from genetically modified pmel mice ($1\text{-}3\times10^7$ freshly isolated pmel splenocytes injected intravenously). In pmel mice, 80% of CD8+ T cells are specific to mgp100 peptide which is known to be expressed in B16 melanoma [116]. Preliminary acute studies demonstrated that each liquefied lesion was approximately 4 mm in length and 0.5 mm in diameter [115]. The focus was therefore scanned in 0.5 mm steps to cover approximately 80% of the tumor volume while monitoring boiling bubble activity by B-mode ultrasound (Figure 8B). The whole tumor volume was not ablated entirely to preserve some of the infiltrating lymphocytes. Animals were sacrificed and tissues (spleen, ipsilateral and contralateral inguinal lymph nodes, blood and tumor) were harvested 2 (n=4) or 7 (n=4) days post treatment, processed and stained with three panels of mAbs (Abcam) for flow cytometry.

It was shown that BH treatment was successfully performed in all cases without disrupting the skin; the tumors were flattened and spread out immediately post treatment, suggesting liquefaction of the tumor. However, the BH exposure did not decrease the rate of subsequent tumor growth, which became pronounced within 2 days after the treatment (Figure 8C). No metastatic lesions were found in any of the animals on necropsy. No statistically significant difference was found between control and treatment groups in the number, activation status and phenotype of the CD8 and CD4 cells in either tissue, neither 2 days nor 7 days after the treatment. However, substantial variability was observed between subjects, and reaching statistical significance under these conditions would only be expected if very pronounced effects occurred. The percentage of the adoptively transferred Thy1.1+CD8+ T cells was very low in all tissues, varying within 0-5% of all CD8+ T cells, which indicated that these tumor-specific CD8 T cells did not preferentially proliferate. On the second day after treatment, the number of activated mature dendritic cells (CD11c+MHCII+CD86+), as well as other lymphocytes bearing MHCII receptor in ipsilateral inguinal lymph node was

elevated in treatment group compared to the sham control group, but this elevation did not reach statistical significance. On the seventh day after treatment, the number of MHCII-bearing lymphocytes in the spleen (likely B cells) was significantly elevated in the treatment group compared to the sham control group.

It was shown therefore that BH treatment of subcutaneous B16 murine melanoma did not appear to boost adaptive anti-tumor immunity in a clinically significant way, even when combined with adoptive immunotherapy. However, substantially elevated numbers of MHCII-bearing lymphocytes in ipsilateral lymph nodes and spleen suggest that macrophages and B cells may play a role in the immune response to this treatment and warrant further investigation. It is also important to note that this study was limited to observation of very pronounced immunologic effects due to the small number of animals per group, as well as large inter-subject variability observed. BH treatment was performed only once, whereas immunotherapies often imply repeated administration of adjuvants. In conclusion, immune response to boiling-histotripsy remains an important open question, and should be addressed using more relevant animal models (e.g. orthotopic or *de novo* tumors).

Tissue Engineering and Regenerative Medicine Application

Tissue loss and organ failure is a costly problem for the U.S. health care system, and standard treatments are far from ideal. Currently, the standard of care for end-stage organ failure is orthotopic transplantation; however, even when a viable donor organ is available there are still concerns over immune failure. A promise of tissue engineering is to develop tissue and organ substitutes that replace diseased or injured tissue and organs. Although there have been some major technological advances in this field, the number of tissue engineered medical devices used clinically are limited and there is still no viable tissue engineered replacement for whole organs.

Suitable replacement tissues require scaffolds to provide three-dimensional support with an appropriate mechanical and biological environment to promote cell attachment, migration, proliferation, and neo-tissue genesis. As such, biomimetic scaffolds have been sought after for this purpose. The complex architecture of native tissue, however, has been hard to recapitulate in the lab setting. The use of mammalian biological scaffolds composed from allogenic or xenogeneic extracellular matrix (ECM) could establish a foundation on which functional replacement of whole organs and complex tissues could be developed. Indeed, such scaffolds have been successfully used in a range of tissue engineering/regenerative medicine applications for thin structures [117, 118]. However, the critical limiting factor in the regeneration of whole organs or even large portions of tissue is the need for a vascular supply [119]. Cells *in vivo* cannot survive more than 200 μm from a vessel due to limitations in diffusion [120-121]. Therefore, without a vascular supply, it is difficult for the cells within implanted tissue to obtain sufficient oxygen and nutrients to survive let alone function properly.

The creation of bioartifical organs by decellularization shows great promise in creating three-dimensional scaffolds with an intact vasculature system that could potentially be rapidly integrated with the recipient’s circulatory system. Decellularization is the process by which the cellular material of an organ/tissue is removed by the application of chemical or

biological agents in combination with mechanical force leaving the matrix intact. The remaining material consists of an innate 3-D structure and native biochemistry. Current decellularization techniques are lengthy processes (days) and can result in chemical alterations of the matrix [122]. Typically, ultrasound has been used to augment chemical or enzymatic decellularization agents [123]. Decellularization using ultrasound alone has been used on thin regions of tissue (up to 500 μm), but without much improvement in time for decellularization [124].

The possibility of using boiling histotripsy for decellularizing large tissue volumes in short time was tested in recent experiments. Freshly excised and degassed bovine liver cubes of 2.5 inch size were exposed to BH using a clinical MR-guided HIFU system [125]. Mechanical lesions of 1 cm diameter in cross-section were generated using electronic steering of the array. The exposure applied 10 ms pulses with duty cycles of 1, 3, or 5 %, *in situ* $p+$= 78 and $p-$=12 MPa. [126].

After treatment, lesions were cut in cross section, photographed, and then rinsed to visualize the remaining structure. The lesion contents were analyzed for protein denaturation using a technique developed in another study [20]. Separate samples were prepared for histological evaluation. Sections from the whole lesions were stained with hematoxylin and eosin (H&E), Picro sirius red, Masson's trichrome or for nicotinamide adenine dinucleotide-diaphorase (NADH-d) activity [20].

Volumetric lesions (1 cm in diameter) were produced in less than 20 minutes. Macroscopic evaluation showed that all lesions contained homogenized tissue with tissue liquefaction being less complete with increasing duty cycle. The lesions formed here were similar to single lesions previously reported in other BH studies [20]. Once the liquid contents were washed from the lesion, a three-dimensional matrix could be seen (Figure 9A). This tissue structure appeared to be pliable and easily manipulated without damage (Figure 9C). Increasing amounts of thermal damage to the tissue was visually evident with increasing duty cycles and this was confirmed NADH-d staining (Figure 9A). Histological evaluation revealed lesions contained intact stroma and patent vessels (Figure 9) surrounded by liquefied cells. However, small caliber vessels (<50 μm) were only observed in the lower duty cycle samples (Figure 9B).

In summary, it was shown that volumetric lesions containing liquefied cells and varying degrees of intact extracellular matrix were formed by BH in a short space of time. A volume that would take traditional decellularization methods days, took under 20 minutes. At a duty cycle of 5%, the integrity of the smaller caliber vessels was difficult to distinguish due to disruption of the tissue. It is possible that the large thermal effect made the small caliber vessels more susceptible to mechanical insult. However, with the lower duty cycles, small vessels (< 50 μm) were observed macroscopically and histologically. These vessels appeared to be patent, which is important for tissue replacement. At these low duty cycles the preserved structure was pliable upon manipulation. Although some damage to collagen was observed in all lesions, the extent of the damage was not evaluated. It is likely that the treatment parameters could be further optimized to result in complete decellularization with minimal connective tissue damage, whilst preserving essential ECM elements. Aside from

the benefit of reduced times for treatment, the ability to decellularize tissue without the need of chemical or biological agents would also be a great advantage of an ultrasound protocol.

These findings suggest that large volumes of liver tissue can be decellularized in a short period of time by boiling histotripsy while leaving essential 3-D tissue structures intact. With further tailoring of the pulsing scheme parameters, this treatment modality could potentially be utilized for the decellularization of organs for tissue engineering and regenerative medicine applications.

Discussion

The descriptions given above for several applications of histotripsy methods are a few examples of what is possible using a mechanical method for tissue disruption. There are several attributes of histotripsy that contribute to its potential. As seen here, both types of histotripsy, although based on different mechanisms, generate similar bioeffects and can be applied to a variety of tissue types. At the same time, histotripsy displays selective ablation, and appears to leave large blood vessels and other structures intact. Pulse sequences such as those used for cavitation cloud histotripsy can also disintegrate kidney stones to very fine particles. Thus, applications include the elimination of any tissue or other material in the body for which the mechanical action of histotripsy would achieve appropriate levels of disintegration or other biological effects. Both methods provide the ability to use ultrasound imaging methods for targeting and monitoring treatments in real time.

The use of low duty factors eliminates the heating of overlying tissues which is a commonly observed side effect for thermal HIFU, where waiting periods are required to diminish tissue heating along the propagation path, resulting in a long total treatment time. Treatment of adjacent focal spots involves propagation through largely the same path and thus accumulation of thermal effects in these tissues. The nonlinearity of the field can enhance the heating preferentially in the focal zone if the pressure amplitude is sufficiently high and if the aperture is large such that the nonlinear distortion of the waveform is limited to the focal zone [11]. This same nonlinearity plays a significant role in boiling histotripsy where enhanced focal heating is necessary and shock scattering for cavitation cloud histotripsy relies on the nonlinearity to produce the high peak positive pressure and high amplitude shock fronts in the focal waveform [18]. However, both of these histotripsy approaches use low duty factors that limit, if not eliminate, heating along the propagation path where nonlinear effects are not yet significant.

As was discussed with regard to applications to the liver when considering the short pulses in cavitation cloud histotripsy, beam side lobes from distorting aberrations can be “thresholded out” if they do not change the shape of the main lobe and the main lobe still exceeds any side lobe (often the case even with severe aberrations). Thus, if the main focal lobe is still extant, and exceeds the intrinsic threshold, a clean bubble cloud and lesion is formed thus conferring significant immunity to aberrations [55, 56]. Under these conditions, one can then produce clean lesions at the targeted site through ribs, skull, and other highly aberrating and attenuating structures. Similarly, shock fronts in acoustic waveforms, necessary for boiling histotripsy, are generated when the *in situ* pressure exceeds some threshold level. Recent simulation studies based on the nonlinear Westevelt equation for the

acoustic field and on the bioheat equation for the temperature field have shown that shock fronts form within the main focal lobe, while only slightly distorted waveforms are present in the side lobes developed [94].

Excellent spatial control of cavitation cloud histotripsy has been demonstrated using a range of ultrasonic frequencies. Spatial control can also be achieved if a high frequency probe waveform, such as an imaging pulse, intersects a low frequency pump waveform in the focus [127]. The compounded waveform can momentarily exceed the intrinsic threshold, thus producing a lesion based on the spatial control achievable with the probe (imaging) transducer. Multi-beam histotripsy allows precise lesions with much smaller transducers where the “heavy lifting” is accomplished with a much lower frequency pump transducer. Such an approach would allow simultaneous imaging with therapy where the imaging pulses could contribute to the therapeutic application, treating precisely where one is imaging. One can then envision future systems where such an approach is taken.

When p_- of the waveform just exceeds the intrinsic threshold, this approach is called microtripsy [14] and the bubble cloud can consist of a single bubble and very small lesions, much less than the diffraction limit in size are formed (Figure 10). This approach provides an extreme level of spatial control of histotripsy. In the short pulse limit, “monopolar” pulses [128] with high p_-, ideal for histotripsy, can be synthesized in a generalization of the multi-beam histotripsy case wherein very short pulses from transducer elements of many different frequencies are added at the focus of what is called a “frequency compounding” transducer. One can think of the monopolar negative pressure pulse as the acoustic waveform shorn of all non-essential features for producing supra-intrinsic threshold histotripsy lesions. Suppression of positive shock fronts reduces unwanted thermal effects due to absorption of higher order harmonics, and reduces the somewhat chaotic effects of shock scattering. So while not useful in boiling histotripsy where harmonics are needed, such monopolar pulses would be effective in cavitation cloud histotripsy and are particularly attractive for microtripsy where the only activation would be for that portion of the waveform that is just beyond the intrinsic threshold. Moreover, this minimalist, very short waveform reduces diffraction aberration effects to a near absolute minimum. With pulses longer than several cycles, such diffraction effects can even result in multiple lesions, even with a single intended focus, when the waveform is propagated through nearly periodic structures like the ribs. Monopolar positive pulses and other “arbitrary” waveforms can also be synthesized by frequency compounding with both therapy and imaging applications. Having the ability to select the polarity of the pulses would allow important mechanistic studies to be conducted.

Several examples have been given here showing the control achievable with histotripsy but we do not yet know everything that controls histotripsy. The nucleation of bubbles could play a role in each type of histotripsy. The nucleation process for the formation of gas bubbles can be considered as heterogeneous or homogeneous. Several potential sources of heterogeneities in fluids have been identified including gas pockets on particles [129, 130], or gas bubbles stabilized with surfactant skins [131] or ionic surface charge stabilized [132]. These heterogeneous nuclei serve to lower an “incidental” threshold for cavitation in fluids and appear in different sizes and number densities, thus leading to spatial and temporal

variations when fluids are subjected to tensile stress, such as by the negative pressure in an ultrasonic wave. If such nuclei were a distribution containing ideal gas bubbles, acoustic cavitation thresholds are predicted in the range of 1 MPa for frequencies in the range of 0.5 – 5 MHz and such thresholds are the origin of the mechanical index (MI) used as an output metric in diagnostic ultrasound [133]. However, the range of pressures that would activate such nuclei could be quite varied depending on this heterogeneous nuclei population. The incidental threshold would be analogous to the incipient threshold, the first observable cavitation threshold, as the ultrasound pressure amplitude is increased for fluids with heterogeneous nuclei. When considering an increasing pressure amplitude field, these heterogeneous nuclei will be activated and if on the axis of the shock wave can be the inception point for the bubble cloud as in the shock scattering approach to histotripsy. In the case of boiling histotripsy, as the tissue at the focus rapidly heats, such nucleation will be increasingly likely at the boiling site.

For homogeneous nucleation, the theoretical limit to the tensile strength can be very high depending on the target medium. For example, if the medium consists of only water molecules, this limit has been estimated as high as 140 MPa [134]. However, even in pure fluids, there are variations in the molecular configurations due to thermal fluctuations, which create temporally transient regions where the tensile strength is reduced [135]. Looking to such limits, there are several publications that place the cavitation threshold for such nuclei sources in the range of 24-33 MPa. Therefore the intrinsic threshold referred to here is this level of cavitation activation where these ubiquitous nuclei are affected.

Conclusions

The preclinical examples of applications presented here give a sample of the potential for this technology. The prospects for more technical advances is continuing with our increasing understanding of the attributes of the different variations of histotripsy and how to control its mechanical effects. Histotripsy can be applied to a wide variety of tissues and materials with spatial control over it effects and selectivity to spare structures such as large vessels. Both ultrasound and MR imaging can be used for targeting and monitoring the treatment in real time. Three different pulse length regimes result in different mechanisms for tissue disruption while having some of the same advantages such as elimination of heating effect as a consequence of the low time average power used. Clinical translation of histotripsy methods will depend on many factors such as safety and efficacy, displacement of existing methodologies and physician acceptance but the preclinical results seen thus far warrant the continued investigation of histotripsy as a potentially disruptive technology for noninvasive surgery.

Acknowledgements

The authors, as a part of large teams at the University of Michigan, the University of Washington, and Moscow State University, would like to acknowledge many students, postdoctoral fellows, researchers, and collaborators, who have contributed to the development of histotripsy methods. This work was supported by the National Institute of Health (R01 DK091267, EB007643, EB008998, CA134579; P01DK043881, K01EB015745, T32DK007779), the Russian Science Foundation (14-12-00974), the American Cancer Society (RSG-13-101-01-CCE), the Hartwell Foundation, the Focus Ultrasound Foundation, and NSBRI through NASA NCC 9-58.

References

1. Dubinsky TJ, Cuevas C, Dighe MK, Kolokythas O, Hwang JH. High-intensity focused ultrasound: Current potential and oncologic applications. AJR Am J Roentgenol. 2008; 190(1):191–199. [PubMed: 18094311]
2. Kim YS, Kim JH, Rhim H, Lim HK, Keserci B, Bae DS, et al. Volumetric MR-guided high-intensity focused ultrasound ablation with a one-layer strategy to treat large uterine fibroids: initial clinical outcomes. Radiology. 2012; 263(2):600–609. [PubMed: 22403170]
3. Crouzet S, Chapelon JY, Rouvière O, Mege-Lechevallier F, Colombel M, Tonoli-Catez H, et al. Whole-gland ablation of localized prostate cancer with high-intensity focused ultrasound: oncologic outcomes and morbidity in 1002 patients. Eur Urol. 2014; 65(5):907–914. [PubMed: 23669165]
4. Illing RO, Kennedy JE, Wu F, ter Haar GR, Protheroe AS, Friend PJ, et al. The safety and feasibility of extracorporeal high-intensity focused ultrasound (HIFU) for the treatment of liver and kidney tumours in a western population. Br J Cancer. 2005; 93:890–895. [PubMed: 16189519]
5. Wu F, Wang ZB, Chen WZ, Wang W, Gui Y, Zhang M, et al. Extracorporeal high intensity focused ultrasound ablation in the treatment of 1038 patients with solid carcinomas in China: An overview. Ultrason Sonochem. 2004; 11:149–154. [PubMed: 15081972]
6. Napoli A, Anzidei M, Marincola BC, Brachetti G, Ciolina F, Cartocci G, et al. Primary pain palliation and local tumor control in bone metastases treated with magnetic resonance-guided focused ultrasound. Invest Radiol. 2013; 48(6):351–358. [PubMed: 23571832]
7. Elias WJ, Huss D, Voss T, Loomba J, Khaled M, Zadicario E, et al. A pilot study of focused ultrasound thalamotomy for essential tremor. N Engl J Med. 2013; 369(7):640–648. [PubMed: 23944301]
8. Coluccia D, Fandino J, Schwyzer L, O'Gorma R, Remonda R, Martins E, et al. First non-invasive thermal ablation of a brain tumor with MR guided focused ultrasound. J Neurol Surg A Cent Eur Neurosurg. 2014; 75:p50.
9. Hall, TL.; Fowlkes, JB.; Cain, CA. Imaging feedback of tissue liquefaction (histotripsy) in ultrasound surgery; 2005 IEEE Ultrasonics Symposium; Rotterdam. 2005.
10. Canney, M.; Khokhlova, V.; Hwang, JH.; Khokhlova, T.; Bailey, M.; Crum, L. Tissue erosion using shock wave heating and millisecond boiling in high intensity ultrasound field; Proc. 9th International Symposium on Therapeutic Ultrasound; 2009. p. 36-39.
11. Bailey MR, Khokhlova VA, Sapozhnikov OA, Kargl SG, Crum LA. Physical mechanisms of the therapeutic effect of ultrasound. Acoust Phys. 2003; 49(4):369–388.
12. Parsons JE, Cain CA, Abrams GD, Fowlkes JB. Pulsed cavitational ultrasound therapy for controlled tissue homogenization. Ultrasound Med Biol. 2006; 32(1):115–129. [PubMed: 16364803]
13. Maxwell AD, Cain CA, Hall TL, Fowlkes JB, Xu Z. Probability of cavitation for single ultrasound pulses applied to tissues and tissue-mimicking materials. Ultrasound Med Biol. 2013; 39(3):449–65. [PubMed: 23380152]
14. Lin KW, Kim Y, Maxwell A, Wang TY, Hall T, Xu Z, et al. Histotripsy beyond the intrinsic cavitation threshold using very short ultrasound pulses: Microtripsy. IEEE Trans Ultrason Ferroelectr Freq Control. 2014; 61(2):251–265. [PubMed: 24474132]
15. Maxwell AD, Wang TY, Cain CA, Fowlkes JB, Sapozhnikov OA, Bailey MR, et al. Cavitation clouds created by shock scattering from bubbles during histotripsy. J Acoust Soc Am. 2011; 130(4):1888–1898. [PubMed: 21973343]
16. Khokhlova TD, Canney MS, Khokhlova VA, Sapozhnikov OA, Crum LA, Bailey MR. Controlled tissue emulsification produced by high intensity focused ultrasound shock waves and millisecond boiling. J Acoust Soc Am. 2011; 130(5):3498–510. [PubMed: 22088025]
17. Canney MS, Bailey MR, Crum LA, Khokhlova VA, Sapozhnikov OA. Acoustic characterization of high intensity focused ultrasound fields: A combined measurement and modeling approach. J Acoust Soc Am. 2008; 124(4):2406–2420. [PubMed: 19062878]
18. Canney MS, Khokhlova VA, Bessonova OV, Bailey MR, Crum LA. Shock-induced heating and millisecond boiling in gels and tissue due to high intensity focused ultrasound. Ultrasound Med Biol. 2010; 36(2):250–267. [PubMed: 20018433]

19. Simon JC, Sapozhnikov OA, Khokhlova VA, Wang YN, Crum LA, Bailey MR. Ultrasonic atomization of tissue and its role in tissue fractionation by high intensity focused ultrasound. Phys Med Biol. 2012; 57(23):8061–8078. [PubMed: 23159812]
20. Wang YN, Khokhlova T, Bailey M, Hwang JH, Khokhlova V. Histological and biochemical analysis of mechanical and thermal bioeffects in boiling histotripsy lesions induced by high intensity focused ultrasound. Ultrasound Med Biol. 2013; 39(3):424–438. [PubMed: 23312958]
21. Khokhlova TD, Wang YN, Simon JC, Cunitz BW, Starr F, Paun M, et al. Ultrasound-guided tissue fractionation by high intensity focused ultrasound in an in vivo porcine liver model. Proc Natl Acad Sci U S A. 2014; 111(22):8161–8166. [PubMed: 24843132]
22. Maxwell A, Sapozhnikov O, Bailey M, Crum L, Xu Z, Fowlkes B, et al. Disintegration of tissue using high intensity focused ultrasound: Two approaches that utilize shock waves. Acoustics Today. 2012; 8(4):24–36.
23. Barry MJ, Fowler FJ Jr, O'Leary MP, Bruskewitz RC, Holtgrewe HL, Menust WK, et al. The American Urological Association symptom index for benign prostatic hyperplasia: The Measurement Committee of the American Urological Association. J Urol. 1992; 148:1549–1557. [PubMed: 1279218]
24. Roehrborn, CG.; McConnell, JD. Etiology, pathophysiology, epidemiology, and natural history of BPH. In: Walsh, PC.; Retik, AB.; Vaughan, ED., Jr.; Wein, AJ., editors. Campbell's Urology. W. B. Saunders Co.; Philadelphia: 2002.
25. Berry SJ, Coffey DS, Walsh PC, Ewing LL. The development of human benign prostatic hyperplasia with age. J Urol. 1984; 132:474–479. [PubMed: 6206240]
26. Wei JT, Calhoun E, Jacobsen SJ. Urologic diseases in America project: Benign prostatic hyperplasia. J Urol. 2005; 173:1256–1261. [PubMed: 15758764]
27. Mebust WK, Holtgrewe HL, Cockett ATK, Peters PC. Transurethral prostatectomy: Immediate and postoperative complications. A cooperative study of thirteen participating institutions evaluating 3,885 patients. J Urol. 1989; 141:243–247. [PubMed: 2643719]
28. Roos NP, Wennberg JE, Malenka DJ, Fisher ES, McPherson K, Andersen TF, et al. Mortality and reoperation after open and transurethral resection of the prostate for benign prostatic hyperplasia. N Engl J Med. 1989; 320:1120–1123. [PubMed: 2469015]
29. Lake AM, Hall TL, Kieran K, Fowlkes JB, Cain CA, Roberts WW. Histotripsy: minimally invasive technology for prostate tissue ablation in an in vivo canine model. Urology. 2008; 72:682–686. [PubMed: 18342918]
30. Hall TL, Hempel CR, Wojno K, et al. Histotripsy of the prostate: dose effects in a chronic canine model. Urology. 2009; 74:932–937. [PubMed: 19628261]
31. Schade GR, Hall TL, Roberts WW. Urethral-sparing histotripsy of the prostate in a canine model. Urology. 2012; 80:730–735. [PubMed: 22840869]
32. Wheat JC, Hall TL, Hempel CR, Cain CA, Xu Z, Roberts WW. Prostate histotripsy in an anticoagulated model. Urology. 2010; 75:207–211. [PubMed: 19931897]
33. Firth AM, Haldane SL. Development of a scale to evaluate postoperative pain in dogs. J Am Vet Med Assoc. 1999; 214:651–659. [PubMed: 10088012]
34. Hempel CR, Hall TL, Cain CA, Fowlkes JB, Xu Z, Roberts WW. Histotripsy fractionation of prostate tissue: local effects and systemic response in a canine model. J Urol. 2011; 185:1484–1489. [PubMed: 21334667]
35. Styn N, Hall TL, Fowlkes JB, Cain CA, Roberts WW. Histotripsy homogenization of the prostate: thresholds for cavitation damage of periprostatic structures. J Endourol. 2011; 25:1531–1535. [PubMed: 21815807]
36. Allam C, Wilkinson JE, Cheng X, Ives KA, Hall TL, Roberts WW. Histotripsy effects on the bladder trigone: functional and histologic consequences in the canine model. J Endourol. 2013; 27:1267–1271. [PubMed: 23731213]
37. Schade GR, Keller J, Ives K, Cheng X, Rosol TJ, Keller E, et al. Histotripsy focal ablation of implanted prostate tumor in an ACE-1 canine cancer model. J Urol. 2012; 188:1957–1964. [PubMed: 22999534]
38. Bosch FX, Ribes J, Diaz M, Cleries R. Primary liver cancer: Worldwide incidence and trends. Gastroenterology. 2004; 127:S5–S16. [PubMed: 15508102]

39. Pelletier SJ, Fu S, Thyagarajan V, Romero-Marrero C, Batheja MJ, Punch JD, et al. An intention-to-treat analysis of liver transplantation for hepatocellular carcinoma using organ procurement transplant network data. Liver Transpl. 2009; 15:859–868. [PubMed: 19642139]
40. Livraghi T, Makisalo H, Line PD. Treatment options in hepatocellular carcinoma today. Scand J Surg. 2011; 100:22–29. [PubMed: 21482502]
41. Boutros C, Somasundar P, Garrean S, Saied A, Espat NJ. Microwave coagulation therapy for hepatic tumors: Review of the literature and critical analysis. Surg Oncol. 2010; 19:e22–32. [PubMed: 19268571]
42. Gage AA, Baust JG. Cryosurgery for tumors. J Am Coll Surg. 2007; 205:342–356. [PubMed: 17660083]
43. Dick EA, Taylor-Robinson SD, Thomas HC, Gedroyc WM. Ablative therapy for liver tumours. Gut. 2002; 50:733–739. [PubMed: 11950826]
44. Kudo M. Radiofrequency ablation for hepatocellular carcinoma: updated review in 2010. Oncology. 2010; 78(Suppl 1):113–124. [PubMed: 20616593]
45. McWilliams JP, Yamamoto S, Raman SS, Loh CT, Lee EW, Liu DM, et al. Percutaneous ablation of hepatocellular carcinoma: current status. J Vasc Interv Radiol. 2010; 21(8 Suppl):S204–213. [PubMed: 20656230]
46. Al-Bataineh O, Jenne J, Huber P. Clinical and future applications of high intensity focused ultrasound in cancer. Cancer Treat Rev. 2012; 38(5):346–353. [PubMed: 21924838]
47. Okada A, Murakami T, Mikami K, Onishi H, Tanigawa N, Marukawa T, et al. A case of hepatocellular carcinoma treated by MR-guided focused ultrasound ablation with respiratory gating. Magn Reson Med Sci. 2006; 5(3):167–171. [PubMed: 17139143]
48. Jung SE, Cho SH, Jang JH, Han JY. High-intensity focused ultrasound ablation in hepatic and pancreatic cancer: Complications. Abdom Imaging. 2011; 36:185–195. [PubMed: 20512487]
49. Hall, TL.; Lee, GR.; Hernandez, L.; Cain, CA. Relaxation properties of cavitation induced tissue lesions; Joint Annual Meeting of the International Society for Magnetic Resonance in Medicine; 2007.
50. Wang TY, Xu Z, Winterroth F, Hall TL, Fowlkes JB, Rothman ED, et al. Quantitative ultrasound backscatter for pulsed cavitational ultrasound therapy- histotripsy. IEEE Trans Ultrason Ferroelectr Freq Control. 2009; 56:995–1005. [PubMed: 19750596]
51. Bobkova S, Gavrilov L, Khokhlova V, Shaw A, Hand J. Focusing of high-intensity ultrasound through the rib cage using a therapeutic random phased array. Ultrasound Med Biol. 2010; 36:888–906. [PubMed: 20510186]
52. Khokhlova VA, Bobkova SM, Gavrilov LR. Focus splitting associated with propagation of focused ultrasound through the rib cage. Acoust Phys. 2010; 56:665–674. [PubMed: 21607120]
53. Wang H, Ebbini E, O'Donnell M, Cain CA. Phase abberation correction and motion compensation for ultrasonic phased arrays: Experimental results. IEEE Trans Ultrason Ferroelectr Freq Control. 1994; 41(1):34–43.
54. Kim Y, Wang TY, Xu Z, Cain CA. Lesion generation through ribs using histotripsy therapy without aberration correction. IEEE Trans Ultrason Ferroelectr Freq Control. 2011; 58:2334–2343. [PubMed: 22083767]
55. Kim Y, Vlaisavljevich E, Owens GE, Allen SP, Cain CA, Xu Z. In vivo transcostal histotripsy therapy without aberration correction. Phys Med Biol. 2014; 59:2553–2568. [PubMed: 24785433]
56. Vlaisavljevich E, Kim Y, Allen S, Owens G, Pelletier S, Cain C, et al. Image-guided non-invasive ultrasound liver ablation using histotripsy: Feasibility study in an in vivo porcine model. Ultrasound Med Biol. 2013; 39:1398–1409. [PubMed: 23683406]
57. Vlaisavljevich E, Kim Y, Owens G, Roberts W, Cain C, Xu Z. Effects of tissue mechanical properties on susceptibility to histotripsy-induced tissue damage. Phys Med Biol. 2014; 59:253–270. [PubMed: 24351722]
58. Bulger C, Jacobs C, Patel N. Epidemiology of acute deep vein thrombosis. Tech Vasc Interv Radiol. 2004; 7:50–54. [PubMed: 15252760]
59. Goldhaber SZ. Pulmonary embolism. N Engl J Med. 1998; 339:93–104. [PubMed: 9654541]
60. Rogers LQ, Lutcher CL. Streptokinase therapy for deep vein thrombosis: A comprehensive review of the english literature. Am J Med. 1990; 88:389–395. [PubMed: 2183600]

61. Sharafuddin MJ, Sun S, Hoballah JJ, Youness FM, Sharp WJ, Roh BS. Endovascular management of venous thrombotic and occlusive diseases of the lower extremities. J Vasc Interv Radiol. 2003; 14:405–423. [PubMed: 12682198]
62. Meunier J, Holland C, Lindsell C, Shaw G. Duty cycle dependence of ultrasound enhanced thrombolysis in a human clot model. Ultrasound Med Biol. 2007; 33:576–583. [PubMed: 17337113]
63. Parikh S, Motarjeme A, McNamara T, Raabe R, Hagspiel K, Benenati JF, et al. Ultrasound-accelerated thrombolysis for the treatment of deep vein thrombosis: Initial clinical experience. J vasc interv radiol. 2008; 19:521–528. [PubMed: 18375296]
64. Rosenschein U, Furman V, Kerner E, Fabian I, Bernheim J, Eshel Y. Ultrasound imaging-guided noninvasive ultrasound thrombolysis: Preclinical results. Circulation. 2000; 102:238–245. [PubMed: 10889137]
65. Wright C, Hynynen K, Goertz D. In vitro and in vivo high-intensity focused ultrasound thrombolysis. Invest Radiol. 2012; 47:217–225. [PubMed: 22373533]
66. Deng CX, Xu Q, Apfel RE, Holland CK. In vitro measurements of inertial cavitation thresholds in human blood. Ultrasound Med Biol. 1996; 22:939–948. [PubMed: 8923712]
67. Daniels S, Kodama T, Price DJ. Damage to red blood cells induced by acoustic cavitation. Ultrasound Med Biol. 1995; 21:113–119. [PubMed: 7754571]
68. Kieran K, Hall TL, Parsons JE, Wolf JS Jr, Fowlkes JB, Cain CA, et al. Refining histotripsy: Defining the parameter space for the creation of nonthermal lesions with high intensity, pulsed focused ultrasound of the in vitro kidney. J Urol. 2007; 178:672–676. [PubMed: 17574617]
69. Xu Z, Fowlkes JB, Ludomirsky A, Cain CA. Investigation of intensity thresholds for ultrasound tissue erosion. Ultrasound Med Biol. 2005; 31:1673–1682. [PubMed: 16344129]
70. Xu Z, Fan Z, Hall TL, Winterroth F, Fowlkes JB, Cain CA. Size measurement of tissue debris particles generated from pulsed ultrasound cavitational therapy - histotripsy. Ultrasound Med Biol. 2009; 35:245–255. [PubMed: 19027218]
71. Maxwell AD, Cain CA, Duryea AP, Yuan L, Gurm HS, Xu Z. Noninvasive thrombolysis using pulsed ultrasound cavitation therapy - histotripsy. Ultrasound Med Biol. 2009; 35:1982–1994. [PubMed: 19854563]
72. Maxwell AD, Owens G, Gurm HS, Ives K, Myers DD Jr. Xu Z. Noninvasive treatment of deep venous thrombosis using pulsed ultrasound cavitation therapy (histotripsy) in a porcine model. J Vasc Interv Radiol. 2011; 22:369–377. [PubMed: 21194969]
73. Maxwell AD, Park S, Vaughan BL, Cain CA, Grotberg JB, Xu Z. Trapping of embolic particles in a vessel phantom by cavitation-enhanced acoustic streaming. Phys Med Biol. 2014; 59:4927–4943. [PubMed: 25109407]
74. Park S, Maxwell AD, Owens GE, Gurm HS, Cain CA, Xu Z. Non-invasive embolus trap using histotripsy-an acoustic parameter study. Ultrasound Med. Biol. 2013; 39:611–619. [PubMed: 23415285]
75. Xu Z, Fowlkes JB, Rothman ED, Levin AM, Cain CA. Controlled ultrasound tissue erosion: The role of dynamic interaction between insonation and microbubble activity. J Acoust Soc Am. 2005; 117:424–435. [PubMed: 15704435]
76. Ryan LK, Foster FS. Tissue equivalent vessel phantom for intravascular ultrasound. Ultrasound Med Biol. 1997; 23:261–273. [PubMed: 9140183]
77. Scales CD Jr, Smith AC, Hanley JM, Saigal CS. Prevalence of kidney stones in the United States. Eur Urol. 2012; 62:160–165. [PubMed: 22498635]
78. Mobley TB, Myers DA, Grine WB, Jenkins JM, Jordan WR. Low energy lithotripsy with the Lithostar: treatment results with 19,962 renal and ureteral calculi. J Urol. 1993; 149(6):1419–1424. [PubMed: 8501779]
79. Liston TG, Montgomery BS, Bultitude MI, Tiptaft RC. Extracorporeal shock wave lithotripsy with the Storz Modulith SL20: the first 500 patients. Br J Urol. 1992; 69(5):465–469. [PubMed: 1623372]
80. Coz F, Orvieto M, Bustos M, Lyng R, Stein C, Hinrichs A, et al. Extracorporeal shockwave lithotripsy of 2000 urinary calculi with the modulith SL-20: success and failure according to size and location of stones. J Endourol. 2000; 14(3):239–246. [PubMed: 10795612]

81. Pishchalnikov YA, Sapozhnikov OA, Bailey MR, Williams JC Jr, Cleveland RO, Colonius T, et al. Cavitation bubble cluster activity in the breakage of kidney stones by lithotripter shockwaves. J Endourol. 2003; 17(7):435–46. [PubMed: 14565872]
82. Duryea AP, Hall TL, Maxwell AD, Xu Z, Cain CA, Roberts WW. Histotripsy erosion of model urinary calculi. J Endourol. 2011; 25(2):341–344. [PubMed: 21091223]
83. Zhu S, Cocks FH, Preminger GM, Zhong P. The role of stress waves and cavitation in stone comminution in shock wave lithotripsy. Ultrasound Med Biol. 2002; 28(5):661–671. [PubMed: 12079703]
84. Duryea AP, Roberts WW, Cain CA, Tamaddoni HA, Hall TL. Acoustic bubble removal to enhance SWL efficacy at high shock rate: An in vitro study. J Endourol. 2014; 28(1):90–95. [PubMed: 23957846]
85. Duryea AP, Roberts WW, Cain CA, Hall TL. Removal of residual nuclei to enhance histotripsy kidney stone erosion at high rate. J Acoust Soc Am. 2014; 136:2193.
86. Delius M. Minimal static excess pressure minimises the effect of extracorporeal shock waves on cells and reduces it on gallstones. Ultrasound Med Biol. 1997; 23(4):611–617. [PubMed: 9232770]
87. Zhong P, Zhou Y. Suppression of large intraluminal bubble expansion in shock wave lithotripsy without compromising stone comminution: methodology and in vitro experiments. J Acoust Soc Am. 2001; 110(6):3283–91. [PubMed: 11785829]
88. Bailey MR, Blackstock DT, Cleveland RO, Crum LA. Comparison of electrohydraulic lithotripters with rigid and pressure-release ellipsoidal reflectors. II. Cavitation fields. J Acoust Soc Am. 1999; 106(2):1149–1160. [PubMed: 10462818]
89. Xi X, Zhong P. Improvement of stone fragmentation during shock-wave lithotripsy using a combined EH/PEAA shock-wave generator-in vitro experiments. Ultrasound Med Biol. 2000; 26(3):457–467. [PubMed: 10773377]
90. Wang TY, Xu Z, Hall T, Fowlkes J, Roberts W, Cain C. Active focal zone sharpening for high-precision treatment using histotripsy. IEEE Trans Ultrason Ferroelectr Freq Control. 2011; 58(2): 305–15. [PubMed: 21342816]
91. Maxwell, AD.; Kreider, W.; Yuldashev, PV.; Khokhlova, TD.; Sapozhnikov, OA.; Bailey, MR., et al. A boiling histotripsy system for deep tissue ablation; Conference Program and abstracts of the 13th International Symposium for Therapeutic Ultrasound (ISTU 2013); p. 131
92. Bessonova OV, Khokhlova VA, Canney MS, Bailey MR, Crum LA. A derating method for therapeutic applications of high intensity focused ultrasound. Acoust Phys. 2010; 56(3):376–385.
93. Duck, F. Physical properties of tissue: A comprehensive reference book. Academic Press; London: 1990.
94. Yuldashev PV, Shmeleva SM, Ilyin SA, Sapozhnikov OA, Gavrilov LR, Khokhlova VA. The role of acoustic nonlinearity in tissue heating behind a rib cage using high intensity focused ultrasound phased array. Phys Med Biol. 2013; 58(8):2537–2559. [PubMed: 23528338]
95. Siegel R, Naishadham D, Jemal A. Cancer statistics, 2013. CA Cancer J Clin. 2013; 63(1):11–30. [PubMed: 23335087]
96. Kane CJ, Mallin K, Ritchey J, Cooperberg MR, Carroll PR. Renal cell cancer stage migration: analysis of the National Cancer Data Base. Cancer. 2008; 113(1):78–83. [PubMed: 18491376]
97. Campbell SC, Novick AC, Belldegrun A, et al. Guideline for management of the clinical T1 renal mass. J Urol. 2009; 182(4):1271–1279. [PubMed: 19683266]
98. Zargar H, Allaf M, Bhayani S, Stifelman M, Rogers C, Ball M, et al. Trifecta and Optimal Peri-operative outcomes of Robotic and Laparoscopic Partial Nephrectomy In Surgical Treatment Of Small Renal Masses: A Multi-Institutional Study. BJU Int. Sep 15.2014 Epub ahead of print.
99. Psutka SP, Feldman AS, McDougal WS, McGovern FJ, Mueller P, Gervais DA. Long-term oncologic outcomes after radiofrequency ablation for T1 renal cell carcinoma. Eur Urol. 2013; 63(3):486–492. [PubMed: 22959191]
100. Marberger M, Schatzl G, Cranston D, Kennedy JE. Extracorporeal ablation of renal tumours with high-intensity focused ultrasound. BJU Int. 2005; 95(Suppl 2):52–55. [PubMed: 15720335]

101. Ritchie RW, Leslie T, Phillips R, Wu F, Illing R, ter Haar G, et al. Extracorporeal high intensity focused ultrasound for renal tumours: a 3-year follow-up. BJU Int. 2010; 106(7):1004–1009. [PubMed: 20230379]
102. Roberts WW, Hall TL, Ives K, Wolf JS, Fowlkes JB, Cain CA. Pulsed cavitational ultrasound: a noninvasive technology for controlled tissue ablation (histotripsy) in the rabbit kidney. J Urol. 2006; 175(2):734–738. [PubMed: 16407041]
103. Hall TL, Kieran K, Ives K, Fowlkes JB, Cain CA, Roberts WW. Histotripsy of rabbit renal tissue in vivo: temporal histologic trends. J Endourol. 2007; 21(10):1159–1166. [PubMed: 17949317]
104. Lake AM, Xu Z, Wilkinson JE, Cain CA, Roberts WW. Renal ablation by histotripsy--does it spare the collecting system? J Urol. 2008; 179(3):1150–1154. [PubMed: 18206166]
105. Styn NR, Wheat JC, Hall TL, Roberts WW. Histotripsy of VX-2 tumor implanted in a renal rabbit model. J Endourol. 2010; 24(7):1145–1150. [PubMed: 20575696]
106. Schade GR, Maxwell AD, Khokhlova TD, Wang YN, Sapozhnikov OA, Bailey MR, et al. Boiling histotripsy of the kidney: Preliminary studies and predictors of treatment effectiveness. J Acoust Soc Am. 2014; 136(4):2251. Pt.2.
107. Wu F, Zhou L, Chen WR. Host antitumour immune responses to HIFU ablation. Int J Hyperthermia. 2007; 23(2):165–171. [PubMed: 17578340]
108. Xia JZ, Xie FL, Ran LF, Xie XP, Fan YM, Wu F. High-intensity focused ultrasound tumor ablation activates autologous tumor-specific cytotoxic T lymphocytes. Ultrasound Med Biol. 2012; 38(8):1363–1371. [PubMed: 22633269]
109. Lu P, Zhu XQ, Xu ZL, Zhou Q, Zhang J, Wu F. Increased infiltration of activated tumor-infiltrating lymphocytes after high intensity focused ultrasound ablation of human breast cancer. Surgery. 2009; 145(3):286–293. [PubMed: 19231581]
110. Dromi SA, Walsh MP, Herby S, Traughber B, Xie J, Sharma KV, et al. Radiofrequency ablation induces antigen-presenting cell infiltration and amplification of weak tumor-induced immunity. Radiology. 2009; 251(1):58–66. [PubMed: 19251937]
111. Wissniowski TT, Hänsler J, Neureiter D, Frieser M, Schaber S, Esslinger B, et al. Activation of tumor-specific T lymphocytes by radio-frequency ablation of the VX2 hepatoma in rabbits. Cancer Res. 2003; 63(19):6496–500. [PubMed: 14559842]
112. Hu Z, Yang XY, Liu Y, Sankin GN, Pua EC, Morse MA, Lyerly HK, et al. Investigation of HIFU-induced anti-tumor immunity in a murine tumor model. J Transl Med. 2007; 11:5–34.
113. Xing Y, Lu X, Pua EC, Zhong P. The effect of high intensity focused ultrasound treatment on metastases in a murine melanoma model. Biochem Biophys Res Commun. 2008; 375(4):645–650. [PubMed: 18727919]
114. Huang X, Yuan F, Liang M, Lo HW, Shinohara ML, Robertson C, et al. M-HIFU inhibits tumor growth, suppresses STAT3 activity and enhances tumor specific immunity in a transplant tumor model of prostate cancer. PLoS One. 2012; 7(7):e41632. [PubMed: 22911830]
115. Khokhlova TD, Simon JC, Wang YN, Paun P, Starr FL, Khokhlova VA, et al. In vivo tissue emulsification using millisecond boiling induced by high intensity focused ultrasound. J Acoust Soc Am. 2011; 129:2477.
116. Overwijk WW, Theoret MR, Finkelstein SE, Surman DR, de Jong LA, Vyth-Dreese FA, et al. Tumor regression and autoimmunity after reversal of a functionally tolerant state of self-reactive CD8+ T cells. J Exp Med. 2003; 198(4):569–580. [PubMed: 12925674]
117. Wainwright DJ. Use of an acellular allograft dermal matrix (AlloDerm) in the management of full-thickness burns. Burns. 1995; 21(4):243–248. [PubMed: 7662122]
118. Badylak SF. Xenogeneic extracellular matrix as a scaffold for tissue reconstruction. Transpl Immunol. 2004; 12(3-4):367–377. [PubMed: 15157928]
119. Grikscheit TC, Vacanti JP. The history and current status of tissue engineering: The future of pediatric surgery. J Pediatr Surg. 2002; 37:277–288. [PubMed: 11877635]
120. Frerich B, Lindemann N, Kurtz-Hoffmann J, Oertel K. In vitro model of a vascular stroma for the engineering of vascularized tissues. Int J Oral Maxillof. 2001; 30:414–420.
121. Lovett M, Lee K, Edwards A, Kaplan DL. Vascularization strategies for tissue engineering. Tissue Eng Part B Rev. 2009; 15(3):353–370. [PubMed: 19496677]

122. Guyette JP, Gilpin SE, Charest JM, Tapias LF, Ren X, Ott HC. Perfusion decellularization of whole organs. Nat Protoc. 2014; 9(6):1451–1468. [PubMed: 24874812]

123. Crapo PM, Gilbert TW, Badylak SF. An overview of tissue and whole organ decellularization processes. Biomaterials. 2011; 32(12):3233–3243. [PubMed: 21296410]

124. Azhim A, Yamagami K, Muramatsu K, Morimoto Y, Tanaka M. The use of sonication treatment to completely decellularize blood arteries: a pilot study. Conf Proc IEEE Eng Med Biol Soc. 2011; 2011:2468–2471. [PubMed: 22254841]

125. Wang YN, Khokhlova TD, Maxwell AD, Kreider W, Partanen A, Farr N, et al. Tissue decellularization with boiling histotripsy and the potential in regenerative medicine. J Acoust Soc Am. 2014; 136(4):2278. Pt.2.

126. Köhler MO, Mougenot C, Quesson B, Enholm J, Le Bail B, Laurent C, et al. Volumetric HIFU ablation under 3D guidance of rapid MRI thermometry. Med Phys. 2009; 36(8):3521–3535. [PubMed: 19746786]

127. Lin KW, Duryea A, Kim Y, Hall T, Xu Z, Cain C. Dual-beam histotripsy: A low-frequency pump enabling a high-frequency probe for precise lesion formation. IEEE Trans Ultrason Ferroelectr Freq Control. 2014; 61(2):325–340. [PubMed: 24474138]

128. Lin KW, Hall T, McGough R, Xu Z, Cain C. Synthesis of monopolar ultrasound pulses for therapy: The frequency-compounding transducer. IEEE Trans Ultrason Ferroelectr Freq Control. 2014; 61(7):1123–1136. [PubMed: 24960702]

129. Atchley AA. The crevice model of bubble nucleation. J Acoust Soc Am. 1989; 86(3):1065–1084.

130. Harvey E, Barnes K, McElroy W, Whitely A, Pease D, Cooper K. Bubble formation in animals, II. Gas nuclei and their distribution in blood and tissues. J Cell Comp Physiol. 1944; 21:23–34.

131. Yount DE. Skins of varying permeability: A stabilization mechanism for gas cavitation nuclei. J Acoust Soc Am. 1979; 65(6):1429–1439.

132. Vinogradova OI, Bunkin NF, Churaev NV, Kiseleva OA, Lobeyev AV, Ninham BW. Submicrocavity structure of water between hydrophobic and hydrophilic walls as revealed by optical cavitation. Journal of Colloid and Interface Science. 1995; 173(2):443–447.

133. Apfel RE, Holland CK. Gauging the likelihood of cavitation from short-pulse, low-duty cycle diagnostic ultrasound. Ultrasound Med Biol. 1991; 17:179–185. [PubMed: 2053214]

134. Fisher JC. The fracture of fiquids. Journal of Applied Physics. 1948; 19(11):1062–1067.

135. Church CC. Spontaneous homogeneous nucleation, inertial cavitation and the safety of diagnostic ultrasound. Ultrasound Med Biol. 2002; 28(10):1349–1364. [PubMed: 12467862]

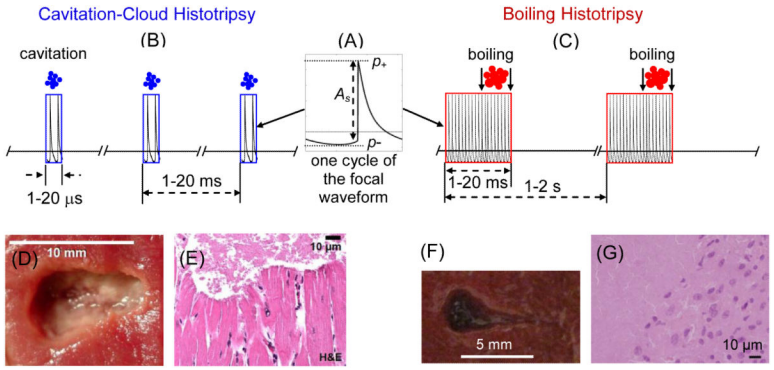

Figure 1.

(A) Highly asymmetric nonlinear pressure waveform with shock fronts at the focus typical for histotripsy. Different pulsing schemes used in (B) cavitation cloud histotripsy and (C) boiling histotripsy approaches; (D) Cavitation cloud histotripsy lesion in ex vivo porcine myocardial muscle. (E) H&E section at boundary of the lesion showing the bisection of myocytes and the complete homogenization of tissue. (After Parson et al. [12]) (F) Boiling histotripsy lesion in ex vivo bovine liver tissue. (G) H&E section through the lesion boundary showing complete disintegration of cells in the lesion.

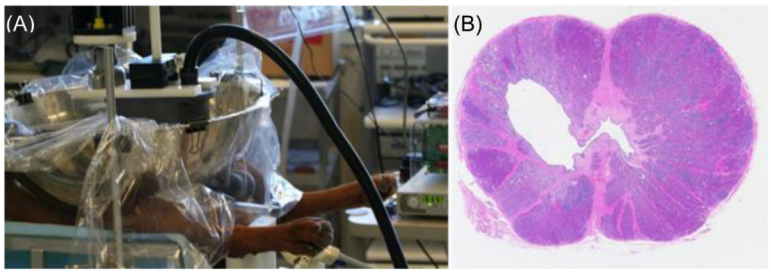

Figure 2.

(A) Histotripsy was applied to the prostate transcutaneously in anesthetized canine subjects. A transrectal ultrasound imaging probe provided real-time visualization of the prostate and cavitation bubble cloud during treatment. (B) H&E stained cross-section of the prostate four weeks after treatment. The targeted volume (devoid of debris) is seen within the glandular prostate communicating with the urethra.

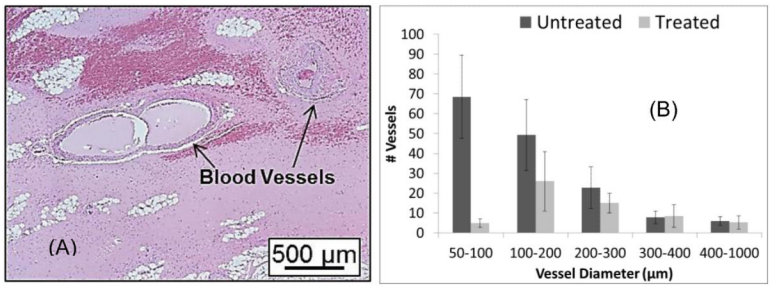

Figure 3.

(A) H&E slide showing intact vessels (indicated by arrows) remained in the completely fractionated liver. (B) There is no statistical significance in the number of vessels above 300μm diameter in the treated and control regions. (This figure is adapted from [52])

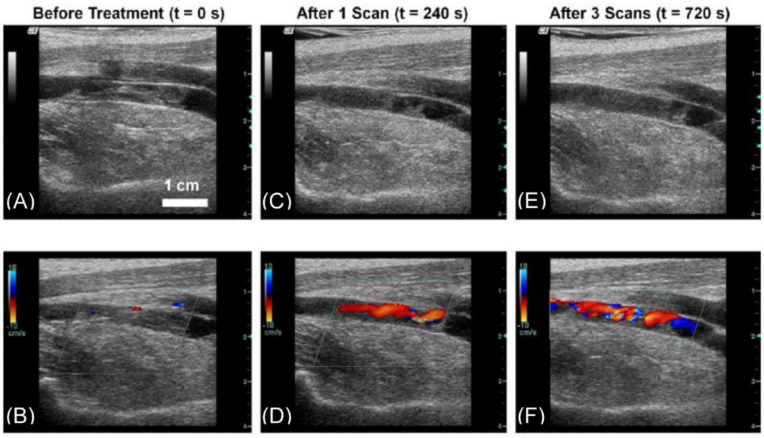

Figure 4.

Ultrasound images of the femoral vein captured by a linear array imaging probe between treatments of a thrombus. (A) and (B) show the original appearance of the vessel on 2D imaging and with color Doppler. (C) and (D) show the thrombus after 240 seconds of treatment (one scan). (E) and (F) show the final condition of the clot after 720 seconds (three scans). Note the decreased echogenicity in the lumen on (C) and (E) compared with (A). Also, a flow channel is clearly visible on (D) and (F), while none was present before treatment in (B). (This figure is adapted from [68])

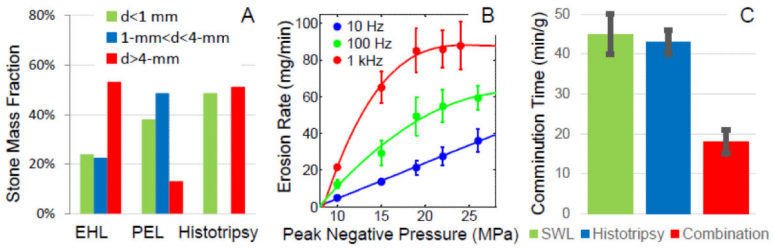

Figure 5.

(A) Fragment size distributions from abbreviated lithotripter and histotripsy treatments. (B) Histotripsy erosion rates for various pulse rates and pressures showing saturation effect. (C) Measured comminution rates for SWL, histotripsy, and combined therapy.

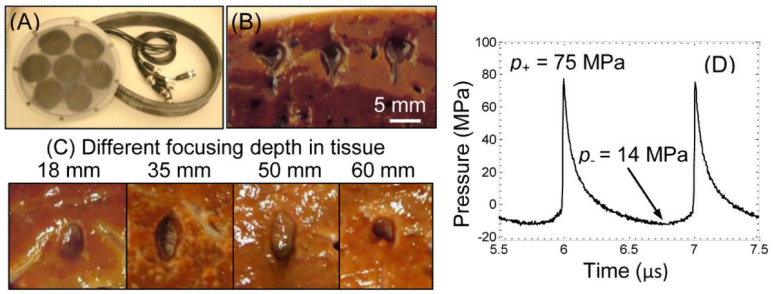

Figure 6.

(A) A boiling histotripsy transducer built to treat through large overlying tissue paths such as liver. (B) Three mechanical lesions generated at shallow depth in ex-vivo bovine liver tissue, showing the tadpole shape. (C) Lesions generated through different liver thicknesses showing consistent dimensions. Ultrasound was generated from the top of the frames. (D) In-situ pressure waveform determined using nonlinear derating method from characterization measurements in water [18, 88].

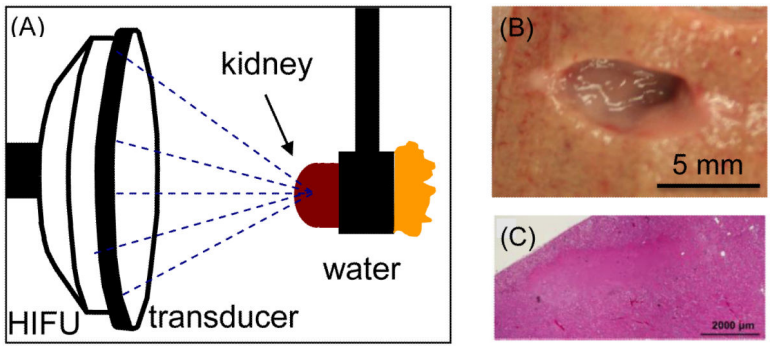

Figure 7.

(A) Experimental set-up for generating boiling histotripsy lesions in ex-vivo porcine kidney. (B) Mechanical lesion in a cortex of the kidney treated with boiling histotripsy. (C) Histologic appearance of a section of boiling histotripsy lesion demonstrating homogenization of the targeted region.

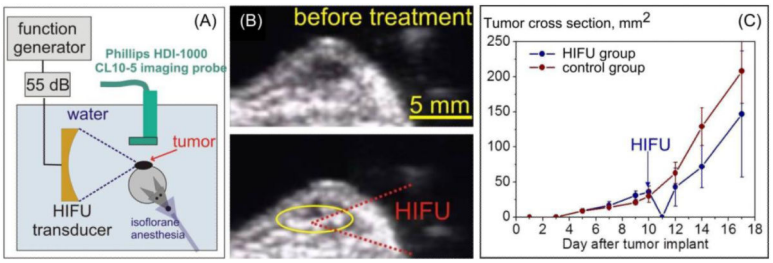

Figure 8.

(A) Diagram of the experimental set-up for boiling histotripsy of subcutaneous B16 melanoma tumors in mice. (B) Frames of B-mode ultrasound recorded before and during boiling-histotripsy treatment of the tumor. (C) The dynamics of the tumor growth before and after boiling histotripsy or sham treatment (n = 4 per group). Although the treatment delayed the tumor growth, it did not affect the subsequent tumor growth rate.

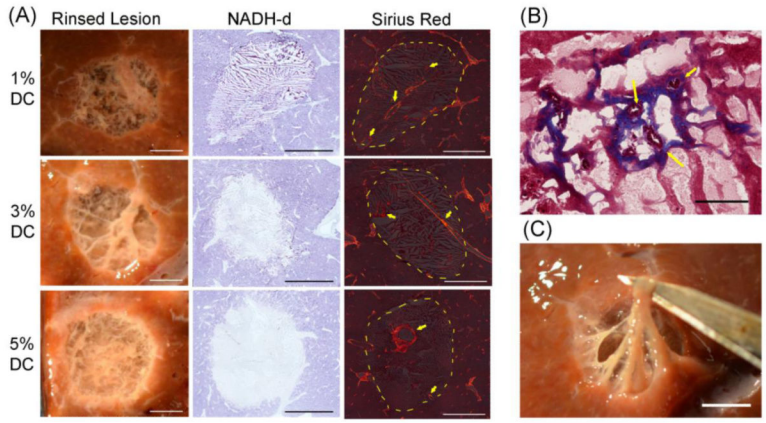

Figure 9.

(A) Photos of boiling histotripsy lesions in ex-vivo bovine liver in cross-section after rinsing (left). Rinsed lesions reveal remaining vasculature and connective tissue that were preserved after sonication. Histomicrographs of representative sections stained with NADH-d (center) and Picro sirius red (right). Unstained regions in the NADH-d stained sections indicate thermal damage. Orange-red birefringence in the Picro sirius red stain sections indicate fibrillar collagen (yellow arrows). Large caliber vessels can be observed to be intact. Dashed yellow line indicates the border of the lesions. Scale bar represents 5 mm. B) Masson's trichome stained sections showing small caliber patent vessels (yellow arrows). Scale bar represents 100 μm. C) Cross section of volumetric lesion with lysed cell debris washed out and with the remaining connective tissue manipulated. Scale bar represents 5mm.

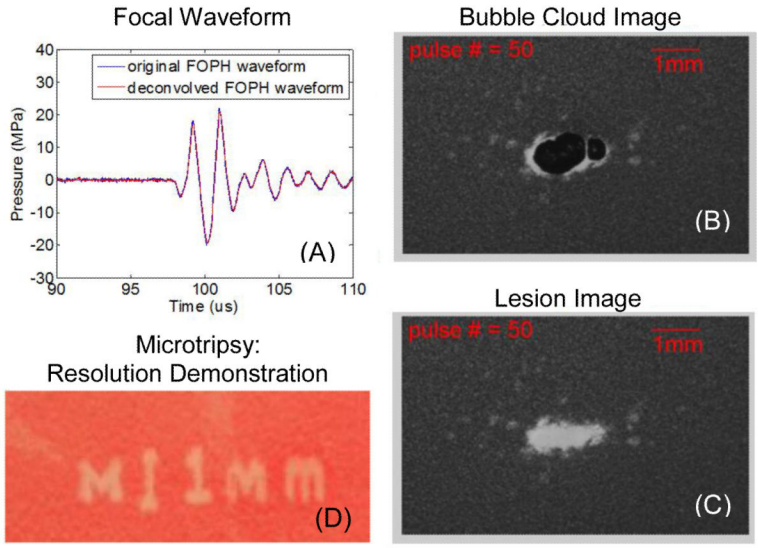

Figure 10.

Microtripsy resulting from a single principal negative half cycle exceeding the intrinsic threshold for cloud cavitation histotripsy. (A) A representative acoustic waveform for a 500 kHz histotripsy pulse measured in water with a fiber optic probe hydrophone (FOPH). (B) Cavitational bubble cloud and (C) corresponding lesion generated in a red blood cell (RBC) phantom using 500 kHz histotripsy pulses with an estimated peak negative pressure of 26.2 MPa (estimated using linear summation). (D) Demonstration of fine spatial resolution as evidenced in the phrase reading “M” (vertical scale bar 1 mm). (Produced using a 3 MHz transducer, and this figure is adapted from Lin et al. [14])